Water management strategies for polymer electrolyte fuel cells (PEFCs) employing microchannel flowfields

Completed by: Simone Daniels

Supervisors: Mr Nabeel Hussain, Dr Shiro Tanaka and Dr Bernhard Schwanitz

Submission of thesis in partial fulfilment of the requirements for a Master of Science Degree

HySA/Catalysis

The Department of Chemical Engineering

University of Cape Town

August 2015

The financial assistance of the National Research Foundation (NRF) towards this research is hereby acknowledged. Opinions expressed and conclusions arrived at, are those of the author and are not necessarily to be attributed to the NRF.

UCT Plagiarism Declaration

1. I know that plagiarism is wrong. Plagiarism is to use another's work and to pretend that it is one's own.

2. I have used UCT Harvard convention for citation and referencing. Each significant contribution to, and quotation in, this project from the work, or works, of other people has been acknowledged through citation and reference.

Name: Simone Daniels

Signature:

Date: 31 August 2015

Synopsis

Polymer electrolyte fuel cells (PEFCs) represent a promising energy conversion technology for automotive and portable applications. In order to achieve the high power densities required for these applications, the fuel cell needs to be operated in the high current density region where the rate of water production is at a maximum. This typically leads to the build-up of liquid water in the porous media and flowfield compartments of the fuel cell. The build-up of liquid water inhibits reactant gas transport to the catalyst layer, leading to a phenomenon called flooding. Flooding causes a rapid drop in cell voltage and is detrimental to fuel cell performance and durability.

Microchannel flowfield designs possess characteristics which could potentially improve water removal from the fuel cell and also reduce the fuel cell system complexity. There is limited knowledge on the use of microchannels flow field designs in PEFCs, specifically how different operating conditions and different membrane electrode assembly (MEA) designs affect the overall performance and water management of a fuel cell using microchannel flow fields. This study investigated two water management strategies for PEFCs employing microchannel flowfields, namely manipulation of operating conditions and modification to the design of components within the MEA.

Four different gas diffusion layer (GDL) cases were tested in a single cell environment at four different cathode flowrates and stoichiometric ratios. The cases consisted of a carbon GDL and three variants of a uniform structured metal GDL. The three metal GDL designs varied in terms of the wettability of the microporous layer coated on the surface of the metal GDL. Several in-situ diagnostic tests, namely polarisation curves, electrochemical impedance spectroscopy (EIS), pressure drop and voltage stability tests were conducted to determine the overall fuel cell performance and water management characteristics of the different GDL cases.

The investigation into the manipulation of operating conditions, specifically an increase in the cathode flowrate, confirmed that this strategy is applicable to a metal GDL-microchannel system as it is for a conventional carbon GDL based system. The sensitivity of a metal GDL system to changes in the cathode flowrate was also found to be similar to the carbon GDL system.

The combination of the results obtained from the diagnostic tests indicated that the uniform structured metal GDL design used in this study significantly improves the water management within the fuel cell. Similar to a carbon GDL system, the wettability of the MPL used in combination with a metal GDL strongly influences the water management within the fuel cell. The best results were observed for an MPL PTFE content of 20 wt%, although the difference performance between 20 wt% and 30 wt% was small in comparison to typical results for carbon GDL systems. This study represents

a first in terms of showing that a metal GDL system performs superior to a carbon GDL system. However it is noted that the result is being obtained when the different GDLs are being used in combination with a microchannel flowfield design.

Overall, an increase in cathode flowrate and specifically the use of a uniform structured metal GDL represent viable water management strategies for fuel cells employing a microchannel flowfield design. A recommendation for further investigations is the use of advanced water imaging methods such as neutron imaging to better understand the reasons for the improved water management of the metal GDL-microchannel flowfield based system.

Acknowledgements

"For wisdom will come into your heart, and knowledge will be pleasant to your soul; discretion will watch over you, understanding will guard you"

Proverbs 2: 10-11

King James Bible

All praise and honour goes first and foremost to the Almighty God. I am humbled by the opportunities he has given to me to further my education and personal development.

A special word of thanks is reserved for my supervisor Nabeel Hussain. His never ending support, guidance, knowledge and insight made this experience both enriching and enjoyable. I am most appreciative for his open door policy and helpful nature.

I would also like to express my thanks to my co-supervisors Dr Shiro Tanaka and Dr Bernhard Schwanitz for sharing their technical and practical knowledge.

I would also like to thinks all the lecturers, research officers and postgraduate students who belong to the Centre for Catalysis Research at the University of Cape Town. Thank you for all the input, big or small, that was given. The friendly, passionate and professional work environment within the group created a stimulating and safe learning environment.

A special thanks to my sponsors, HySA/Catalysis (as part of the Centre for Catalysis Research) as well as the National Research Fund for making this opportunity possible.

Last but not least, I would like to express my thanks to my parents. Words cannot express how grateful I am for the support, patience and strength they have freely given me.

Table of Contents

UCT Plagiarism Declaration i

Synopsis ii

Acknowledgements iv

List of Figures vii

List of Tables ix

Glossary xi

List of Symbols xii

1. Introduction 1

2. Literature Review 2

2.1. Fuel cell technology 2

2.1.1. Fuel cell components 3

Membrane electrode assembly 3

Flowfield 5

2.1.2. Problems with current fuel cell technology 6

2.2. Flooding 7

2.2.1. Description and mechanisms of flooding 7

2.2.2. Impacts of flooding 7

2.3. Water management strategies 8

2.3.1. Manipulation of operating conditions 8

Increasing flow rate 8

Direction of gas flow 9

2.3.2. Flowfield design and properties 9

2.3.3. MEA materials and structure design 11

Catalyst layer 12

Gas diffusion layer 12

2.3.4. Active water management 13

2.4. Fuel cell diagnostic tools 14
2.4.1. Polarisation curves 14
2.4.2. Electrochemical impedance spectroscopy 15
2.5. Characterization of water management 16
2.5.1. Direct techniques 16
Direct visualisation 16
Nuclear magnetic resonance 18
Florescence microscopy 19
Beam interrogation 19
2.5.2. Indirect techniques 20
Pressure drop 20
Residence time distribution 21
Voltage loss 22
2.5.3. Electrochemical techniques 23
3. Objective of study 26
4. Experimental 28
4.1. Experimental cases 28
4.2. Preparation and application of MPL 28
4.3. Fuel Cell Assembly 29
4.3.1. Description of single cell components 29
4.3.2. Assembly procedure 31
4.4. Fuel cell testing 32
4.4.1. Fuel cell start-up procedure 32
4.4.2. Diagnostic tests 34
Overview of fuel cell tests and operating conditions 34
Polarisation curves 34
EIS 35
Two-phase pressure drop coefficient test 35

Voltage stability tests 35
Cathode stoichiometry investigation 36
5. Results and Discussion 38
5.1. Manipulation of operating conditions: effect of varying cathode flowrate 38
5.2. MEA Materials and structure design: Metal GDL 40
5.2.1. Effect of varying cathode flowrate for metal GDL cases 41
5.2.2. Electrochemical Impedance Spectroscopy 44
5.2.3. Two-phase pressure drop coefficient 51
5.2.4. Voltage stability tests 53
6. Conclusions 56
7. Reference 57
8. Appendix 63
8.1. Appendix 1 63
8.2. Appendix 2 64
8.2.1. Sample calculations 64
Calculations used to determine the feed volumetric flow of Hydrogen gas required 64
Calculations used to determine the feed volumetric flow of Air required 64

List of Figures

Figure 1: Schematic diagram of a single PEFC (Lee et al., 1999) 2
Figure 2: Schematic diagram depicting the arrangement of various components used to form the MEA [adapted from Ali et al. (2009)] 4
Figure 3: Schematic of water behaviour in a PEFC (Bhatt et al., 2012) 6
Figure 4: Schematic showing the various locations in a PEFC where flooding can occur (Kumbur & Mench, 2009) 7
Figure 5: Polarisation curves showing fuel cell performance at various air flowrates (Barbir, 2005) 8
Figure 6: Direction of anode and cathode gas flow when operating using A - Co-flow B - Cross-flow and C- Counter-flow (Alaefour et al., 2011) 9

Figure 7: Typical flowfield designs: (A) the conventional flowfield, (B) the serpentine flowfield and (C) the interdigitated flowfield (Wood et al., 1998) 10
Figure 8: Expanded schematic view of a 25cm^2 fuel cell system with a carbon porous wick and electro-osmotic pump (Litster et al., 2007) 14
Figure 9: Magnified view of the various flow mechanisms and patterns in the channels of a PEFC and their corresponding line illustrations showing the form and distribution of liquid water (Hussaini and Wang, 2009) 17
Figure 10: Schematic of the residence time distribution system used (Diep et al., 2007) 22
Figure 11: Typical Nyquist plot of a fuel cell with the equivalent Randles circuit (Chang et al., 2014) 24
Figure 12: Nyquist plotting depicting fuel cell operation normal, flooded and dried conditions (Gebregergis et al., 2010) 25
Figure 13: Assembled single cell fixture and flowfield plate 31
Figure 14: (A) Tools used to compress the cell (B) Tightening pattern at each torque setting 32
Figure 15: Effect of varying cathode flowrate on polarisation curve performance for a carbon GDL system (Test 1) 39
Figure 16: Effect of varying cathode back pressure at a constant cathode flowrate for the carbon GDL system. The result for a higher cathode flowrate is superimposed to discern the influence of increased oxygen partial pressure and increased drag force (Test 9) 40
Figure 17: Effect of varying cathode flowrate on polarisation curve performance for a metal GDL with an MPL containing 15 wt% PTFE (Test 3) 41
Figure 18: Effect of varying cathode flowrate on polarisation curve performance for a metal GDL with an MPL containing 20 wt% PTFE (Test 4) 42
Figure 19: Effect of varying cathode flowrate on polarisation curve performance for a metal GDL with an MPL containing 30 wt% PTFE (Test 5) 42
Figure 20: Comparison of limiting currents for the different MEA component designs at varying cathode flowrates 43
Figure 21: Nyquist Plot for carbon GDL at 0.25 A·cm^{-2} 45
Figure 22: Nyquist Plot for Metal GDL with 15wt% PTFE MPL at 0.25 A·cm^{-2} 45
Figure 23: Nyquist Plot for Metal GDL with 20wt% PTFE MPL 3 at 0.25 A·cm^{-2} 45
Figure 24: Nyquist Plot for Metal GDL with 30 wt% PTFE MPL at 0.25 A·cm^{-2} 45
Figure 25: Comparison of ohmic resistances for all cases as a function of cathode flowrate at 0.25 A·cm^{-2} 46
Figure 26: Comparison of charge transfer resistances for all cases as a function of cathode flowrate at 0.25 A·cm^{-2} 47

Figure 27: Nyquist Plot for carbon GDL at 1.2 A·cm^{-2} 48
Figure 28: Nyquist Plot for Metal GDL with 15wt% PTFE MPL at 1.2 A·cm^{-2} 48
Figure 29: Nyquist Plot for Metal GDL with 20wt% PTFE MPL 3 at 1.2 A·cm^{-2} 48
Figure 30: Nyquist Plot for Metal GDL with 20wt% PTFE MPL 3 at 1.2 A·cm^{-2} 48
Figure 31: Comparison of ohmic resistances for all cases as a function of cathode flowrate at 1.2 A·cm^{-2} 49
Figure 32: Comparison of charge transfer resistances for all cases as a function of cathode flowrate at 1.2 A·cm^{-2} 50
Figure 33: Pressure drop coefficient as function of cathode stoichiometric ratio and current density for carbon GDL 52
Figure 34: Pressure drop coefficient as function of cathode stoichiometric ratio and current density for Metal GDL with 15wt% PTFE MPL 52
Figure 35: Pressure drop coefficient as function of cathode stoichiometric ratio and current density for Metal GDL with 20wt% PTFE MPL 52
Figure 36: Pressure drop coefficient as function of cathode stoichiometric ratio and current density for Metal GDL with 30wt% PTFE MPL 52
Figure 37: Cell voltage at different cathode stoichiometric ratios for carbon GDL at 0.25 A·cm^{-2} 54
Figure 38: Cell voltage at different cathode stoichiometric ratios for Metal GDL with 15wt% PTFE MPL at 0.25 A·cm^{-2} 54
Figure 39: Cell voltage at different cathode stoichiometric ratios for Metal GDL with 20wt% PTFE MPL at 0.25 A·cm^{-2} 54
Figure 40: Cell voltage at different cathode stoichiometric ratios for Metal GDL with 30wt% PTFE MPL at 0.25 A·cm^{-2} 54
Figure 41: Cell voltage at different cathode stoichiometric ratios for carbon GDL at 1 A·cm^{-2} 55
Figure 42: Cell voltage at different cathode stoichiometric ratios for Metal GDL with 15wt% PTFE MPL 1 A·cm^{-2} 55
Figure 43: Cell voltage at different cathode stoichiometric ratios for Metal GDL with 20wt% PTFE MPL at 1 A·cm^{-2} 55
Figure 44: Cell voltage at different cathode stoichiometric ratios for Metal GDL with 30wt% PTFE MPL at 1 A·cm-2 55

List of Tables

Table 1: Summary of the various cases investigated 28
Table 2: Recipes used for MPL fabrication for the various cases tested 29

Table 3: Description of single cell components 30
Table 4: Operating conditions used for fuel cell conditioning cycles 33
Table 5: Summary of tests and operating conditions 34
Table 6: Summary of the average partial pressures of oxygen and exit pressures used for Test 9 36
Table A1: Summary of the various cases investigated 63
Table A2: Summary of tests and operating conditions 63

Glossary

AC	Alternating current
CCM	Catalyst coated membrane
CL	Catalyst layer
EIS	Electrochemical impedance spectroscopy
GDE	Gas diffusion electrode
GDL	Gas diffusion layer
MEA	Membrane electrode assembly
MPL	Microporous layer
OVC	Open circuit voltage
PEFC	Polymer electrolyte fuel cell
PTFE	Polytetrafluoroethylene

List of Symbols

Symbol	Description
P	Absolute pressure (bara)
A	Active area (cm^2)
R_{ct}	Charger transfer resistance ($m\Omega \cdot cm^2$)
I	Current (A)
i	Current density ($A \cdot cm^{-2}$)
F	Faraday's constant ($C \cdot mol^{-1}$)
R	Ideal gas constant ($J \cdot K^{-1} \cdot mol^{-1}$)
$\dot{n_x}$	Moles of species x ($mol \cdot s^{-1}$)
R_Ω	Ohmic resistance ($m\Omega \cdot cm^2$)
RH	Relative humidity (%)
T	Temperature (°C)
$\emptyset_{2P}$	Two phase pressure drop coefficient (-)
V	Voltage (V)
$\dot{V}_X$	Volumetric flowrate of species X ($l \cdot min^{-1}$)

1. Introduction

The polymer electrolyte fuel cell (PEFC) represents a low emission, potentially sustainable alternative energy conversion system for portable, stationery and automotive applications. PEFCs have low operational temperatures, high power density and quick start-up making it advantageous when compared to other fuel cell technologies (Ji & Wei, 2009). Despite these advantages, factors such as cost of components and fuel cell durability exist as the major barriers to the large scale commercialization of this technology. In order to overcome these barriers, innovative ideas and solutions regarding fuel cell material and component development are required.

In order for PEFCs to be viable for automotive and portable applications, the fuel cell systems need to be able to provide sufficient power while satisfying the strict space limitations imposed by the system design. In order to achieve this, the fuel cell needs to be operated in the high current density region. In this region, the rate of liquid water production is at a maximum and this can potentially lead to the build-up of liquid water in the catalyst layer, gas diffusion layer and flowfield compartments of the fuel cell. The build-up of liquid water prevents reactant gases from reaching the catalyst layer, leading to a phenomenon called flooding. Flooding causes a rapid drop in cell voltage and is detrimental to fuel cell performance.

This study will investigate and develop water management strategies for PEFCs employing microchannel flowfields. More specifically, this study will investigate the effect of manipulating operating conditions as well as changing material components on fuel cell performance and cell resistances due to flooding. Furthermore, the study aims to develop a better understanding of the two phase flow patterns in PEFCs and contribute towards the development of PEFCs with improved performance, durability and reduced losses due to fuel cell flooding.

2. Literature Review

This section of the study presents a critical analysis of the relevant literature. It includes an overview of fuel cell technology, a detailed description of fuel cell flooding and water management strategies and a review of the current methods used to characterise water transport and management in the PEFC.

2.1. Fuel cell technology

A fuel cell is an electrochemical device which is able to convert the chemical energy stored in a fuel directly into electrical energy. Hydrogen is the preferred fuel source as it results in the highest theoretical efficiency and power density. The main by-products of a fuel cell are typically water and heat. Depending on the type of fuel cell being used, carbon dioxide may also be formed (Baker & Zhang, 2011).

A fuel cell consists of an anode and cathode compartment which is separated by an electrolyte. Fuel cells are typically classified according the electrolyte used. The PEFC employs a solid polymer membrane as the electrolyte and has a theoretical efficiency of 83% (Barbir & Yazici, 2007). This efficiency typically drops to approximately 50% during normal fuel cell operation. PEFCs are ideal for portable, stationery and transport applications as they have a low operating temperature, a high power density and have the ability for quick start-up.

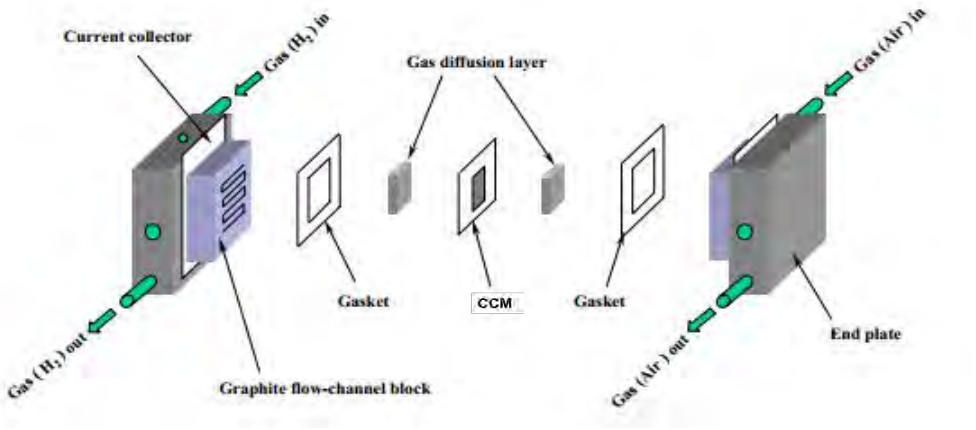

Figure 1: Schematic diagram of a single PEFC (Lee et al., 1999)

Figure 1 shows a schematic diagram of a single PEFC. Hydrogen enters at the anode side of the fuel cell and then moves towards the anode electrode or catalyst layer (CL) by diffusing through the gas diffusion layer (GDL). Once the hydrogen molecules reach the CL it reacts according to the oxidation reaction shown in equation (1). The protons formed in equation (1) pass through the selectively

permeable membrane to the cathode compartment. The electrons are passed through an external circuit from the anode to the cathode resulting in an external current.

$$H_2 \rightarrow 2H^+ + 2\bar{e} \quad (1)$$

During this procedure, oxygen is simultaneously being fed into the cathode side where it is reduced according to the reaction shown in equation (2). This reaction leads to the formation of water on the cathode side of the fuel cell. This water is then ejected from the PEFC by the flow of unreacted oxygen (Barbir, 2006).

$$\frac{1}{2}O_2 + 2H^+ + 2\bar{e} \rightarrow H_2O + heat \quad (2)$$

The overall reaction which occurs across the cell can be seen in (3).

$$H_2 + \frac{1}{2}O_2 \rightarrow H_2O + heat \quad (3)$$

The maximum calculated theoretical voltage which can be achieved by a single hydrogen fuel cell at 25°C and atmospheric pressure is 1.23V (Barbir, 2006). At normal current densities the operating cell voltage can be approximated at 0.6V. The difference between the theoretical and operating voltage is due to the losses that occur within the fuel cell. More specifically, these are the activation, ohmic and mass transfer losses of the cell (Baker & Zhang, 2011).

Cell voltage output can be increase by connecting single fuel cells in series to form a fuel cell stack. Since one of the by-products of a fuel cell is heat, cooling plates are incorporated in the stack design to help control the temperature of the stack. This cooling can be carried out by either air or liquid cooling (Baker & Zhang, 2011).

2.1.1. Fuel cell components

Membrane electrode assembly

One of the important constituents of a PEFC is a five layered structure called the membrane electrode assembly (MEA). The different layers in the MEA consist of a proton exchange membrane, two CLs and two GDLs. These layers are arranged as shown in Figure 2.

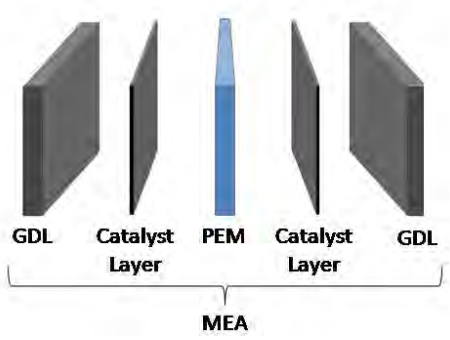

Figure 2: Schematic diagram depicting the arrangement of various components used to form the MEA [adapted from Ali et al. (2009)]

PEFCs use a solid polymer membrane which is impermeable to gases and only allows for the transport of protons from the anode compartment to the cathode compartment of the cell. Proton conduction in the membrane requires the membrane remain hydrated (Barbir, 2006).

A platinum based catalyst being used in the CL is currently the best catalyst available for both the anode and cathode reactions (Baker & Zhang, 2011). Since only the surface catalyst particles are used as active sites for the reaction, platinum nanoparticles are typically supported on carbon support. This minimizes the platinum required which significantly decreases the catalyst cost.

The GDL is located between the CL and a flowfield plate. The main functions of the GDL are to distribute the reactant gases and provide electronic and thermal conductivity. It also helps to remove product water from the catalyst layer (Barbir, 2006). The absence of the GDL from the MEA would result in an accumulation of water in the fuel cell. This accumulation of water hinders the transport of gasses and blocks the catalyst area available for reaction. For this reason, the porosity of the GDL is a vital component in the performance of the fuel cell. The GDL also provides mechanical support for the MEA (Barbir, 2006).

A dual-layer GDL is most commonly used in current PEFC designs. This consists of a thin macro-porous layer consisting of either carbon cloth or carbon paper. This is in direct contact with the gas flow channel. To improve the performance of the fuel cell a microporous layer (MPL), containing carbon powder and a hydrophobic/hydrophilic agent, is applied to the GDL (Park et al., 2012). The macro-porous layer and the MPL together form the dual-layer GDL. The MPL is in direct contact with the CL and its main role is to aid with the removal of liquid water from the CL (Barbir, 2006).

Fuels cells currently employ a carbon fiber based material as the GDL. This material is either woven to form carbon cloth or bound with an agent to form carbon paper. Carbon paper is thinner, relatively compressible and more brittle whilst carbon cloth is more flexible and robust (Jayakumar et al., 2014). The conductivity, hydrophobicity, porosity and mass transfer properties of these two materials are

also slightly different. Carbon fibers are widely used as it is stable in an acidic environment, has high gas permeability and is a good electronic conductor (Park, et al., 2012). However, the manufacturing process used to produce these GDL result in a non-uniform structure and large variation in porosity. Since the porous structure within the GDL plays an important role for gas diffusion and water transport, the unstructured nature of the GDL can result in undesired unpredictable performance.

Metal based GDLs have been proposed as a potential GDL alternative due to its improved stability and mechanical strength over wide potential ranges (Park et al., 2012). Various metal based GDL designs have been investigated by Zhang et al. (2008), Fushinobu et al. (2006) and Blanco et al. (2008) and the findings from these studies were very similar. Specifically the metal GDLs showed inferior fuel cell performance in comparison to conventional carbon fibre based GDLs. However, these papers all claimed that the metal GDLs offered several advantages, namely uniform porosity, reduced thickness, improved water management and improved mechanical support. It should be noted that in all the studies previously mentioned, no indication was made as to the type of flowfield design or channel parameters used when testing was conducted and whether or not this would affect the performance or functionality of the metal GDL. Furthermore, no values comparing the resistance of carbon GDLs and metal GDLs under fuel cell conditions was shown.

Flowfield

The flowfield plates, which are located on either side of the MEA, provide flow channels which supply fuel and oxidant gases to the MEA as well as expel the water generated and any unreacted gases. In a fuel cell stack consisting of several single cells, these plates are typically referred to as bipolar plates. This is because in a stack, one side of the bipolar plate acts as the anode while the opposite side of the plate acts as the cathode.

The two main types of materials used for the flowfield plates include graphite or metal. These materials provide the best compromise between the conflicting requirements in an operating fuel cell. Some of the main requirements include:

- Corrosion resistant
- High electronic and thermal conductivity
- Good mechanical strength
- Gas impermeability
- Chemical compatibility (Mehta & Cooper, 2002)

Non-porous graphite has been extensively used as the flowfield material as it is chemically stable and possesses high electrical and thermal conductivity. Natural as well as synthetic graphite has been used.

The disadvantages of this material include its brittle nature and the high cost associated with its manufacture (Mehta & Cooper, 2002).

Metallic materials such as aluminium, iron, stainless steel, titanium and nickel have all been employed as the flowfield material. Metallic flowfield plates offer advantages of (i) a simpler and more cost effective manufacturing process based on stamping or moulding, (ii) high thermal and electrical conductivities, (iii) stronger mechanical strength and therefore thinner sheets can be used. One of the major drawbacks of metallic materials is the limited corrosion resistance in an acidic PEFC environment. The corrosion resistance of metallic flowfields is typically improved through the use of coatings. However, this may give rise to other issues such as pin-hole defects which could lead to local corrosion and metallic ion contamination of the membrane (Li et al*.,* 2008).

2.1.2. Problems with current fuel cell technology

Large-scale commercialization of PEFCs requires lowering of the cost and an increase in the durability of current technologies. One of the major issues impacting the performance and durability of PEFCs is the water management within the cell. Figure 3 shows the different water transport mechanisms in a PEFC. In addition to the different transport mechanisms the water equilibrium obtained depends on several variables. These variables include the reactant humidification, flowfield design and the structural and wetting properties of the GDL and MPL (Bhatt et al., 2012). Water management strategies for PEFCs need to be in place to ensure optimised performance whilst still maintaining overall system simplicity in order to minimise parasitic power losses (Jei & Wei, 2009).

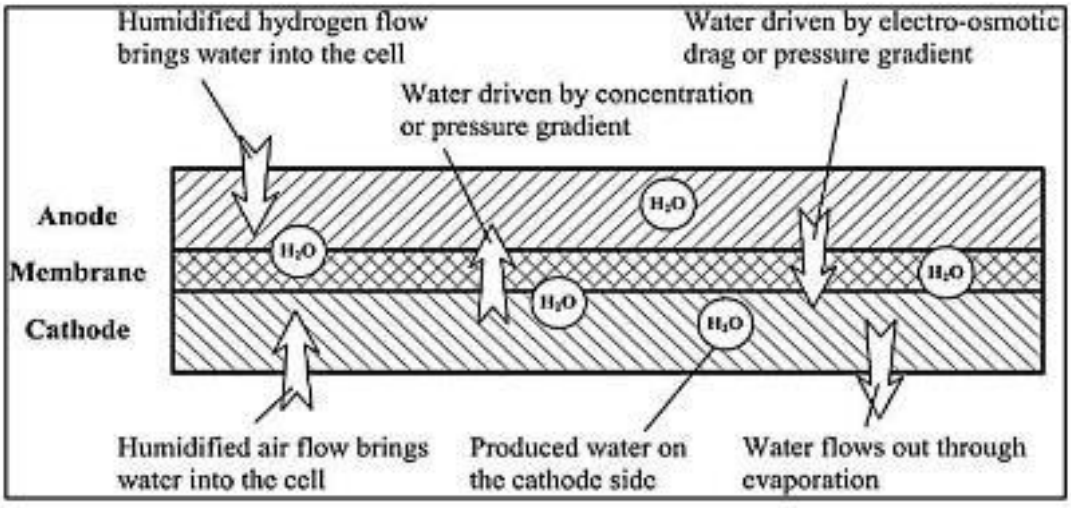

Figure 3: Schematic of water behaviour in a PEFC (Bhatt et al., 2012)

2.2. Flooding

2.2.1. Description and mechanisms of flooding

Figure 4 illustrates the phenomenon of flooding in a fuel cell. Flooding refers to the build-up or accumulation of liquid water on the electrode surface, in the GDL or in gas channels of the flowfield plates. The water accumulation blocks the pathways of the reactant gases to the active catalyst site and negatively affects the performance of the fuel cell. Flooding can occur on both anode and cathode compartments of the cell. Since water is generated at the cathode side of the fuel cell, it is generally more prone to flooding (Ji & Wei, 2009).

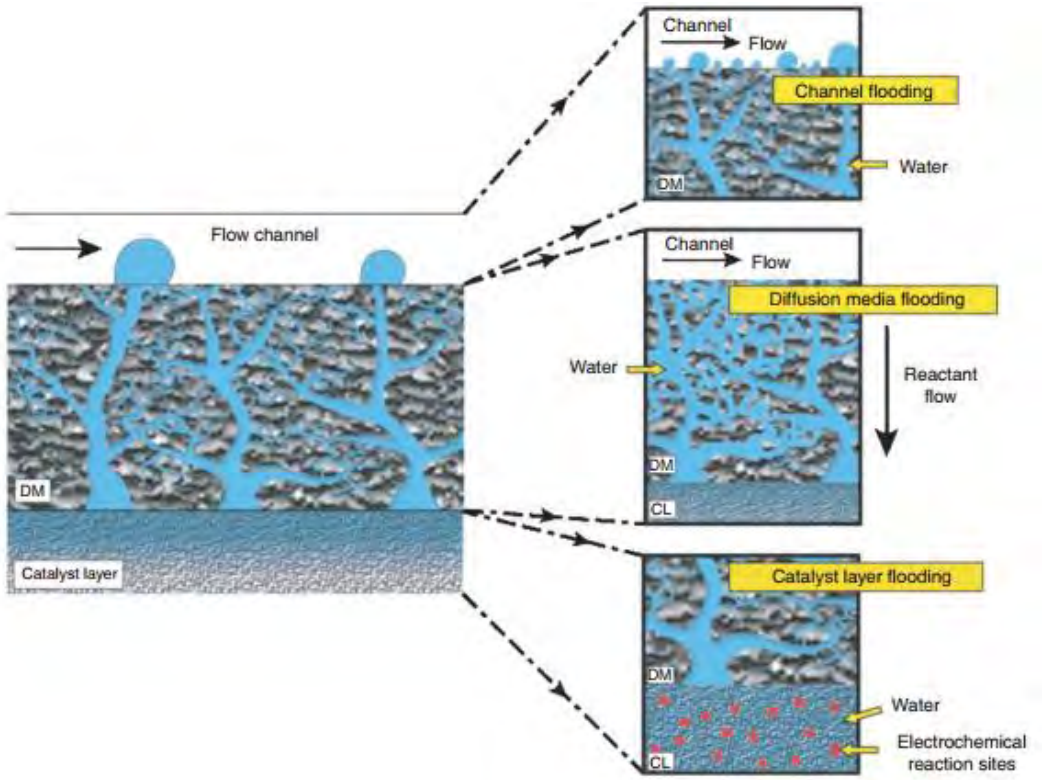

Figure 4: Schematic showing the various locations in a PEFC where flooding can occur (Kumbur & Mench, 2009)

The flooding of an electrode typically occurs during high current density operation where the rate of water production exceeds the rate of water removal from the cell. However, flooding can also occur at low current densities under certain operating conditions. These operating conditions include low temperatures and low gas flowrates. Under these conditions rapid saturation of the gas phase by water vapour occurs causing the cell to flood (Ji & Wei, 2009).

2.2.2. Impacts of flooding

During severe flooding the pathways for reactant gases can be temporarily blocked, giving rise to a rapid drop in cell voltage. Blocked pathways, particularly in the flowfield channels, can result in a

sudden build-up of local pressure that quickly expels the accumulated water from the system, thereby restoring the cell voltage. Build-up of liquid water and the associated pressure build up requires increased parasitic pumping power required to overcome the increased pressure drop in the cell. This in turn results in reduced system efficiency. The intermittent build-up and removal of liquid water in the cell also causes a fluctuation in the cell performance, causing potentially unstable and inconsistent cell performance. Flooding not only compromises the cell performance but also accelerates the degradation of various fuel cell components (Ji & Wei, 2009).

The extent to which water accumulates as well as the effects thereof is strongly dependent upon the operating conditions of the PEFC and the properties of the MEA.

2.3. Water management strategies

Current water management strategies employed for PEFCs can be broadly categorised into four different categories. The categories include: (i) manipulation of operating conditions, (ii) flowfield design and properties, (iii) MEA materials and structure design and (iv) active water management.

2.3.1. Manipulation of operating conditions

Increasing flow rate

According to Babir (2005), higher feed flow rates usually lead to improved fuel cell performance. The increase in fuel cell performance is attributed to both an increase in the concentration of the reactants as well as the improved water removal from the cell by the excess gas flow in the system. An example of the performance improvement is presented in Figure 5.

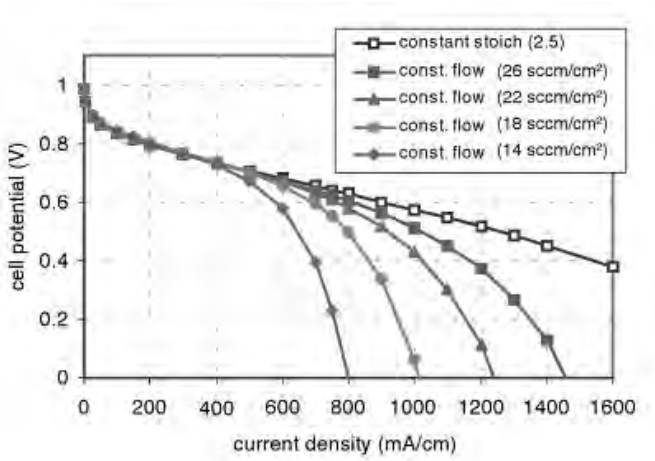

Figure 5: Polarisation curves showing fuel cell performance at various air flowrates (Barbir, 2005)

Whilst this technique is extensively used it has the drawback of increasing the load on the compressor which supplies gases to the fuel cell. The power consumption of the compressor is directly proportional to the flowrate being used (Barbir, 2005). Therefore, while higher flow rates improve fuel

cell performance, increasing the compressor power consumption increases the parasitic power requirements of the system and therefore negatively affects the overall system efficiency (Barbir, 2005).

Direction of gas flow

PEFCs can be operated using either co-, cross- or counter-flow gas arrangements. Figure 6 provides a representation of the gas flow arrangements possible. For the arrangements using co- and counter-flow, the anode and cathode flow channels are arranged in parallel. This allows for gas flow in the same direction for co-flow (Figure 6A) and in the opposite direction for counter-flow (Figure 6C). As seen in Figure 6C, the cross-flow arrangement aligns the two compartments flow channels such that the channels are perpendicular to one another. This ensures that the gas flow direction of the two streams are at right angles from one another (Alaefour et al., 2011).

It has been shown that a counter gas flow configuration results in improved water distribution across the fuel cell (Morin et al., 2010). In co-flow systems, gases on both the anode and cathode typically approach or exceed saturation conditions near the cell exit point. This increases the possibility of condensation near the cell exit. Humidified co-flow systems were found to have better current density distribution when compared to counter-flow systems (Kwac & Kim, 2008). In counter-flow systems, lower inlet humidities can be used since the anode inlet is adjacent to the cathode exit and vice versa (Kwac & Kim, 2008). This reduces the chance of condensation at the fuel cell exit points.

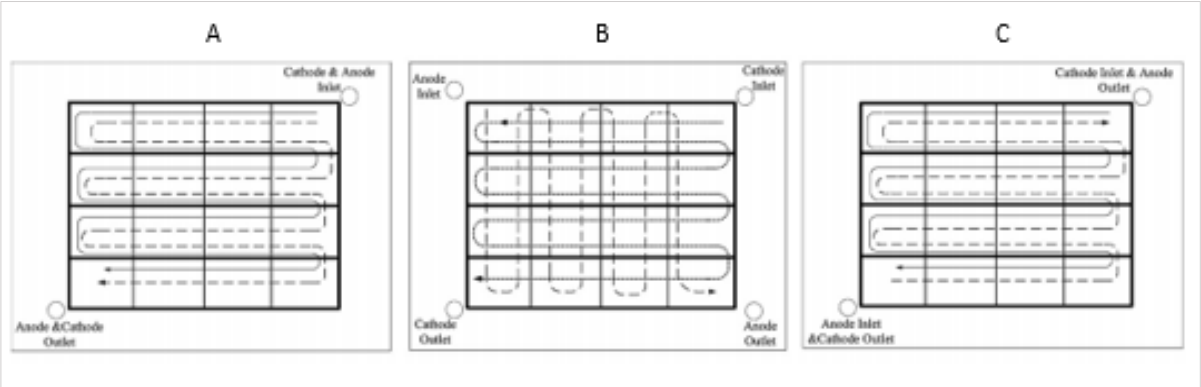

Figure 6: Direction of anode and cathode gas flow when operating using A - Co-flow B - Cross-flow and C- Counter-flow (Alaefour et al., 2011)

2.3.2. Flowfield design and properties

The choice of flowfield design strongly influences the water removal and water balance in the fuel cell. There are three typical flowfield designs currently being used for practical applications. These three

designs are as follows: the conventional parallel flow field, the serpentine flow field and the interdigitated flow field. These flowfield designs can be seen in Figure 7.

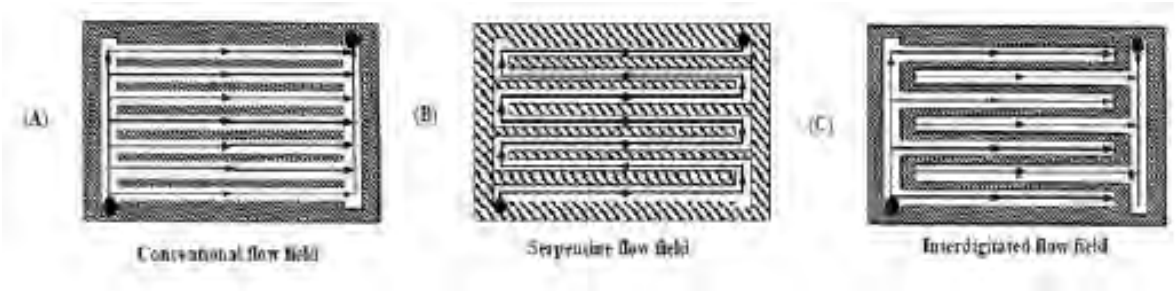

Figure 7: Typical flowfield designs: (A) the conventional flowfield, (B) the serpentine flowfield and (C) the interdigitated flowfield (Wood et al., 1998)

Conventional parallel flowfield designs have been found to be most prone to flooding and are not ideally suited for high humidity or high current density operation ((Nguyen, (1996), (Merida et al., 2006), (Xue & Dong, 1998)). For this flowfield design, the dominant mechanism for the transport of the reactants and products from the flowfield to the CL is diffusion. The pressure drop in conventional parallel channels is not high enough to cause water removal from the channels leading to channel flooding and subsequently flooding in the other layers of the MEA This flowfield design is only appropriate for applications which use high gas flowrates and where a low-pressure drop is needed (Nguyen, 2006).

Serpentine flowfield designs consist of long channels with small cross-sections. The nature of this specific design permits pressure gradients to develop across the porous GDL. This causes cross leakage flow between neighbouring channels. This cross leakage flow induces strong convection in the GDL which transports reactant gases to the CL and simultaneously removes water from the reaction site at the CL and GDL. The serpentine flowfield design is more efficient at water removal than conventional parallel flow field channels, but requires higher inlet pressures of the reactant gases to account for the higher pressure drop (Bhatt et al., 2012).

The interdigitated flow channel design consists of a dead end mode. This forces the gas to flow through the GDL resulting in the convection driven flow of gases through the GDL. The shear force developed from the gas flow pushes out any liquid water in the GDL and reduces the chances of flooding. However the forcing of gas into the GDL result in very high pressure drop and therefore this design, similar to the serpentine design, requires very high inlet pressures which has implications of the overall system efficiency (Bhatt et al., 2012).

Microchannel flowfields have emerged as a possible alternative flowfield design which can be used to improve the water management of the fuel cell. Microchannels, in the context of fuel cell flowfields, are defined as channels with dimensions less than 500 microns. Conventional flowfields typically have channel and land dimensions in the 0.5 – 2 millimetre range. It is believed that the reduction in the channel dimensions reduces liquid water build-up in the GDL and CL under the land section of the flow-field. This in turn will reduce flooding and improve gas dispersion and accessibility to the CL. Whereas some studies have looked into the effects of channel dimensions in the microchannel range (Cha et al., 2006), limited work has been performed to see determine the effect of microchannel flowfields on overall water management in PEFCs. Microchannel flowfields show potential but have yet to be used in conjunction with metal uniform structured GDLs.

In addition to the flowfield design the two-phase flow behaviour in the channels is also affected by hydrophilic/hydrophobic nature of the walls of the channels. Hydrophilic materials typically form liquid water films, while hydrophobic channel surfaces typically form water droplets. Nishida et al. (2015) conducted a study which investigated the effect of channel wettability on a PEFC using a serpentine channel design. This study found that when a high hydrophilic coating was applied to the system where the channels were horizontally positioned, the resultant cathode differential pressure inside the flowfield was lowered. Furthermore, it also prevented water plugging from occurring within the flow channels.

2.3.3. MEA materials and structure design

Membrane

Improved water management has been demonstrated by the use of thinner membranes of approximately 10µm. Thinner membranes reduce the distance for back-diffusion of water, and in doing so reduces the need for anode humidification. Furthermore, thinner membranes improve cell performance by reducing the ohmic losses through the membrane. Thinner membranes are also less sensitive to changes in current density and operating temperature. However, poor durability and higher gas crossover rates are often related to the use of thinner membranes. In order to avoid this, membranes of about 25–40µm are used for fuel cell applications (Freire & Gonzalz, 2001).

In a study conducted by Watanabe et al. (1993) and Watanabe et al. (1996), self-humidifying polymer membranes based on porous wicks, platinum particles and hygroscopic particles were proposed to improve water management when operating with little to no cathode external humidification. Although these membranes showed potential the performance was inferior to conventional membranes.

Catalyst layer

The CL plays a critical role in the water management of a PEFC. The CL influences the extent of conversion of liquid water to vapour and is key to maintaing the balance between the differing water fluxes towards the GDL and membrane (Eikerling & Kornyshev, 1998).

Modification to the microstructure of the CL has been shown to influence water management. A study by Nguyen (2006) looked to reduce the effects of flooding in the CL. They developed a CL structure with multiple interconnected ionic (Nafion) and electronic (Carbon) pathways. These pathways allow for the transport of protons and electrons. This process was followed by partially filling the CL void space with hydrophobic particles. These particles were in the nano-sized range and were placed to provide optimal gas and liquid transport paths to and from the CL. These particles were also required to produce higher ionic and electronic conductivities.

When this procedure was carried out, it was done using two different approaches. The first approach attempted to create a four phased structure. This structure was to include the following phases: gas, liquid, ionic and electronic. The second approach was to investigate the idea of using a starting structure which consisted of three phases (ionic, gas and electronic). This structure was then modified to provide distinct pathways for the gas and liquid phases. Upon comparison of the two approaches, the second approach was favoured and provided a promising stepping stone for future work (Nguyen et al. 2006).

Gas diffusion layer

The GDL plays an important role in water management in a PEFC as it helps maintain the balance between membrane hydration and water removal. The water product formed at the CL is transported to the flowfield channels via the GDL. If a build-up of liquid water occurs in a region with insufficient reactant supply, flooding will occur thus leading to significant mass transfer limitations. To avoid the water accumulation in the porous interstitial spaces, the GDL is often treated with a hydrophobic agent, such as polytetrafluoroethylene (PTFE). This changes the wetting characteristics of the GDL and improves the rate at which water is removed from the system. PTFE treatment results in the formation of both hydrophilic and hydrophobic pockets of pores in the GDL [(Mathias et al., 2003), Gostick et al., (2006)]. These pockets of pore allow for distinct transport pathways for gas and liquid water. PTFE can be loaded into the GDL using various techniques. These techniques spraying, dipping and brushing. PTFE loadings used in literature generally fall in a wide range of between 5 and 30 wt%. The optimum wt% is however strongly dependant on the operating conditions which in turn are driven by the specific fuel cell application.

In addition to the bulk hydrophobic treatment of the GDL, a MPL is often added between the GDL and the CL. This is done to assist in the distribution of the reactant gas to the catalyst surface; increase the contact between the layers and improve the distribution of local current density. However, the most important function of the MPL is to encourage effective transport of liquid water from the CL into the GDL. An MPL usually consists of a mixture of carbon or graphite particles and a polymeric binder (typically PTFE), coated on one side of the GDL, adjacent to the CL. The pore size of MPLs are far smaller (0.1 to 0.5µm) than the pore sizes found in the GDL (10 to 30µm) (Mathias et al., 2003).

A study conducted by Park et al. (2007) looked into the effect of the PTFE concentration in the MPL on PEFC performance. Water permeation, mercury porosimetry and polarisation curve experiments were conducted using carbon substrates coated with MPLs of the following PTFE contents: 10wt%, 20wt%, 30wt% and 40wt%. The water permeation and mercury porosimetry experiments showed that an increase in PTFE led to an increase in the resistance of the water passing through the GDL. This was attributed to a decrease in the porosity of the MPL as well as an increase in the volume of hydrophobic pores. Polarisation curves conducted using oxygen as an oxidant showed that the best fuel cell performance was achieved for a MPL loading of 20wt% (Park et al., 2008). It should be noted that these conclusions drawn were based on tests conducted using pure oxygen as the oxidant. This would not be a complete comparison, as the mass transfer losses would not have been properly compared.

2.3.4. Active water management

Active water management strategies for the context of this study refers to the application of external systems to actively promote water removal in a PEFC. Of all the water management strategies currently available for PEFCs, the information available for this strategy is the most limited and unexplored.

One study which looks at active water management was conducted by Litster et al. (2007). This study presented a system which aimed to decouple the water removal from the delivery of the oxidant. Both active and passive methods were used to assist with water removal. The system used passively distributed water via a porous carbon flowfield plate which acted as an integrated wick. Furthermore, the system also made use of an external electro-osmotic pump to actively drive the excess water from the channels and GDL. Figure 8 shows an expanded view of the components used for this system. Experimental data showed that with the use of an electro-osmotic pump aids robust PEFC operation with a high volumetric power density across all the operating conditions tested in the study. This result was attributed to the improved pressure gradient within the wick enabling the removal of excess water from the system. This enables stable fuel cell operation and assists in a rapid recovery in cases of extreme flooding. Whilst this strategy proved to be successful there additional components add to

system complexity and space so the use of the strategy is strongly driven by the specific application requirements.

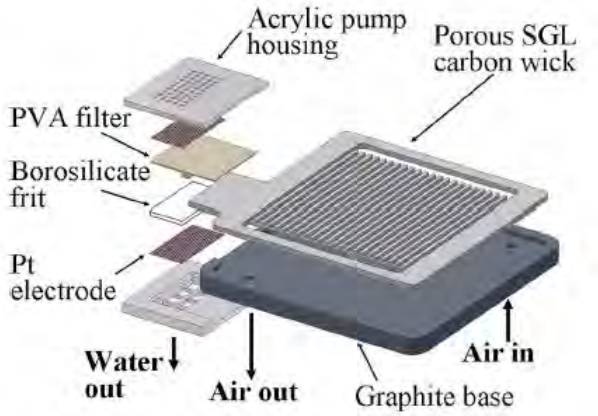

Figure 8: Expanded schematic view of a 25cm^2 fuel cell system with a carbon porous wick and electro-osmotic pump (Litster et al., 2007)

2.4. Fuel cell diagnostic tools

Diagnostic tools used in PEFC research provide an understanding as to fluid, thermodynamics, electrochemical and mechanical processes occurring within the fuel cell.

2.4.1. Polarisation curves

The polarisation curve (PC) the most commonly used in-situ fuel cell diagnostic tool. This curve is generated by measuring the cell voltage as a function of the current density under a particular set of operating conditions. This plot provides an overview of the performance and performance losses of both a single fuel cell and fuel cell stack. Unfortunately, this technique is unable to indicate the performance of individual components within the both the cell or stack. Furthermore, it is also unable to completely differentiate between the various performance losses of the cell. PCs can be used to systematically study the effect of operating parameters such fuel or oxidant composition, flow rate, temperature and relative humidity on overall fuel cell performance.

The PC is generally characterised by three main regions. In each region different performance losses dominate. Activation losses, which are specifically related to the CL properties, are as a result of the sluggish kinetics of the oxygen reduction reaction. These losses are typically dominant at high cell potential and low current densities.

The ohmic losses are typically dominant at intermediate current densities. This type of loss is due to the electrical resistances of each of the components as well as between the components. The resistance to proton conductivity through the membrane is the main contributor to this type of loss.

This is followed by the electric contact resistance between the GDL and the flowfield plates and between the GDL and the CL. In this region of the polarisation curve, the voltage loss generally decreases linearly with increasing current density (Larminie & Dicks, 2003).

Mass transfer losses are dominant at high current densities. This type of loss is due to the transport limitations of the reactant gases in the MEA. The extent of this type of loss is affected by the diffusion and convection of the gases and liquids in the PEFC (Barbir, 2005).

Equation 4 shows the relationship between cell voltage and current density. This equation can be used across the entire current density range being studied (Larminie & Dicks, 2003).

$$E = E_0 - R_i - c\log(i) - l\exp(ni) \quad (4)$$

Where

$$E_0 = E_r + b\log(i_0) \quad (5)$$

E_r	Reversible potential
i_0	Exchange current density
c	Tafel slope for oxygen reduction reaction
l and n	Constants linked to the mass transfer limitations

PCs provide information regarding the overall performance of the cell but are unable to separate the performance of individual cell components and cannot resolve time-dependent processes (Baker & Zhang, 2011). EIS and current interruption are two techniques which can be used to separate these processes.

2.4.2. Electrochemical impedance spectroscopy

Electrochemical impedance spectroscopy (EIS) can be defined as the measure of a system's ability to resist or impede the electrical current applied to it. EIS measurements are conducted by applying an AC current or potential (of known frequency and amplitude) to the fuel cell and analysing responding wave. The amplitude and phase of the resulting signal is measured as a function of frequency. This EIS technique is mainly used to determine the ohmic and transport losses in the cell as well as to assess the cell electrode properties.

The impedance spectra can be described and plotted using either the Bode or Nyquist forms. The Bode plot plots the amplitude and phase of the impedance as a function of frequency, whilst for the Nyquist

plot the imaginary part of the impedance measurement is plotted against the real part at each frequency studied (Li et al., 2008).

The ohmic losses within the MEA can be quantified using the information acquired from the high frequency EIS measurement. The high frequency arc reflects the ohmic resistance, the effective charge transfer resistance and double layer capacitance in the CLs.

2.5. Characterization of water management

Characterisation of water management in PEFCs can be broadly characterised into direct techniques, indirect techniques and electrochemical techniques.

2.5.1. Direct techniques

The effectiveness of water management systems can be evaluated by making use of direct detection techniques which allows one to obtain a visual representation of the liquid water inside an operational fuel cell. Direct water detection techniques that have been used include: direct visualisation (transparent cells), nuclear magnetic resonance (NMR), fluorescence microscopy and beam interrogation.

When considering the various visualization studies conducted on cathode-side channel flooding in literature, the outcomes reported have typically been limited to a qualitative description of flow patterns under a particular set of operating conditions. Direct techniques do not provide a high degree of quantitative information. This is a drawback as quantitative results of two-phase flow patterns and parameters would be more beneficial for materials optimisation and fuel cell stack design purposes. Furthermore, quantitative results would also be useful for experimental validation of multi-physics computational models that take two-phase interactions in gas channels into consideration.

Direct visualisation

Direct visualisation techniques provide high temporal and spatial resolution information about water transport in the GDL pores, gas flow channels and the catalyst surface in an operating fuel cell. The technique requires a transparent cell plate that allows access to the channels for optical devices. These devices include digital camcorders and high-speed cameras, infrared cameras and CCD cameras [(Spernjak et al., 2007)], (Hakenjos et al*.,* 2004)]. The direct visualisation technique cannot however be used to gather information of opaque objects.

Direct visualisation techniques are especially useful for directly observing the effects of operating conditions on water droplet formation, growth and movement (Tüber et al*.*, 2003). This has been shown in a study conducted by Hussaini and Wang (2009). In this study, Hussaini and Wang (2009)

characterized liquid water coverage on cathode GDL and channel flooding by using in-situ visualization of cathode flooding in an operating fuel cell. The fuel cell that was used for testing covered the cathode side of the cell with a transparent Lexan plate. This provided a clear view of the channels of the flowfield. The channels which were used were referred to as microchannels even though the channel dimensions were 10cm in length, 1 mm in width and 0.5mm in depth, which apart from the depth are closer to more conventional channel dimensions.

The results from the study conducted showed that two-phase transport in the channels can occur in the form of droplet, film or slug-flow. These two phase flow mechanisms are preceded by a single-phase mechanism. Figure 9 shows the images obtained for the various mechanisms.

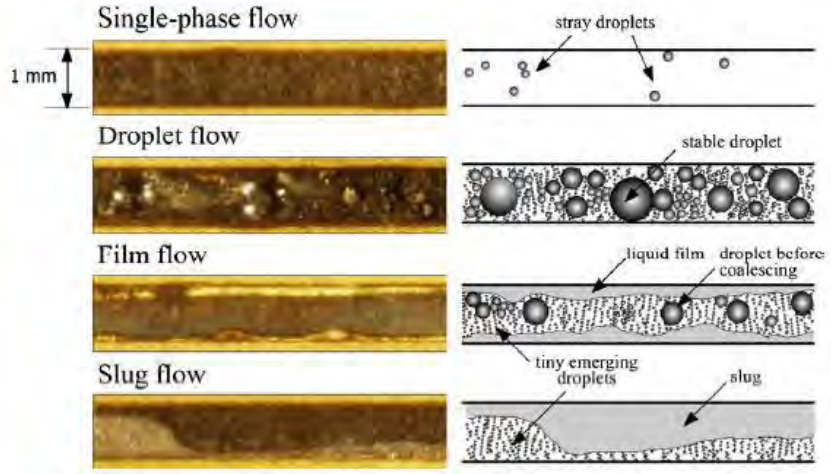

Figure 9: Magnified view of the various flow mechanisms and patterns in the channels of a PEFC and their corresponding line illustrations showing the form and distribution of liquid water (Hussaini and Wang, 2009)

In the single-phase flow regime very few water droplets were observed on the GDL surface and the flow was found to mostly be in the form of partially humidified gas. The water droplets that were intermittently observed on the GDL the surface tended to be rapidly evaporated by the flowing air stream.

The droplets region was dominated by water droplets that emerged from beneath the GDL surface and remained attached to the surface due to surface tension forces. Mass transfer limitations were found to occur at the flowing gas interface. Due to hydrophobic nature of carbon paper GDL surface, droplets were found to be circular in shape and did not spread out laterally on the surface. The maximum droplet radius reached was limited either by its detachment size (under shearing action by gas flow) or the channel depth which was 0.5 mm in this particular case.

In the film flow regime the influx of liquid water through the GDL was found to be sufficiently high so that the water droplets, on contact with either the adjacent droplets or channel walls, coalesce and are wicked into the walls. This formed a liquid film of growing thickness. A wavy motion is observed on the film surface due to the continuous influx of water and coalescence of droplets. Large droplets were no longer observed in this region. Tiny droplets however, may appear and were generally confined to a narrow region at the centre of the channel.

In the slug flow region, further growth of the liquid film was found to cause it to accumulate into a slow-moving slug. This resulted in oscillations in pressure drop and caused an internal adjustment of the flow rate among the channels. Whenever the slugs stagnated in the vicinity of the channel exit, channel clogging occurred. These clogs prevented all gas from passing through it.

These flow patterns which were observed using the direct visualisation technique was of great importance as it provided some of the fundamental information required to model and predict two-phase flow in a PEFC.

As previously mentioned, one of the major drawbacks of direct visualisation techniques for water detection is that it cannot provide quantitative information about the cell. For this particular technique, no quantitative information can be obtained as the technique is limited by the depth perception from the top of the transparent window. Furthermore, this technique is limited by the highly reflective nature of the GDL. Both these limitations make it almost impossible to quantitatively evaluate the volume of water found in the cell (Spernjak et al., 2007).

Nuclear magnetic resonance

Nuclear magnetic resonance (NMR) imaging, also known as magnetic resonance imaging (MRI) is a widely available technique which is by nature three-dimensional. This technique allows for the visualisation of water in opaque structures. Due to these characteristics, the technique has been successfully used to provide in-situ measurements of the liquid water distribution of an operating fuel cell. Furthermore, it has also been successful in showing where liquid can be detected under the gas channel and land areas. This is advantageous when comparing this technique to direct visualisation methods.

Although NMR imaging is capable of providing useful information about the water content in the membranes and gas channels of the cell, it cannot be used to determine the water content in the GDL. This is caused by the rapid break down of the signal produced in the carbon layer (Feindel et al., 2007).

NMR can therefore only be used to observe water in the membrane rather than within paramagnetic materials like carbon. Another disadvantage of this technique is that it has limited temporal and in-plane spatial resolution ((Tsushima et al., 2004), (Bazylak, 2009)).

Florescence microscopy

Fluorescence microscopy in combination with optical photography can be used to visualize the micro-scale transport of liquid water in the GDL surface and the dynamic behaviour of water droplets developing from the GDL into the flowfield (Bazylak et al., 2007). However, due to the GDLs opaque nature, this method cannot be used to explain the full extent of the through-plane transport of the GDL. In addition, the applicability of this method for in situ investigations is not yet unambiguous (Bazylak, 2009). Due to the opaque nature of the GDL material, this technique is limited to a depth of a few GDL fibre diameters. (Bazylak et al., 2007).

Beam interrogation

Two beam interrogation techniques available for water detection include neutron imaging and electron microscopy techniques. These techniques allow the in situ measurement of liquid water distributions in operating PEFCs through materials that would otherwise be opaque when viewed optically (Bazylak, 2009).

The neutron imaging technique for a PEFC is based on the sensitive response of neutrons to compounds containing hydrogen and insensitivity to common fuel cell materials (Feindel et al., 2006). This technique has been acknowledged as being the only diagnostic tool that provides all of the three requirements needed to study the water management in a PEFC. These requirements are as follows: the technique should have *in situ* applicability, should be minimally invasive and should have the ability to provide local information of the cell (Stumper et al., 2005). Even though this technique is very useful, it has limited application because of the high cost associated with this technique. Furthermore, it is also limited by the rare availability of radioactive radiation equipment that provides neutron sources needed for this technique.

Electron microscopy can be used to observe the vapour condensation and liquid water morphology and breakthrough in porous layers of PEFC. In two separate studies conducted by Nam and Kaviany (2003) and Nam et al. (2009), this technique was used to confirm the presence of large droplets and high liquid saturation at the CL and GDL interface. This was due to a jump in pore size. From the studies conducted they were also able to show that there was a reduction in both the droplet size and liquid saturation when making use of an MPL.

2.5.2. Indirect techniques

Indirect water detection techniques rely on the analysis of externally measurable parameters to provide information related to the nature of two-phase flow within the cell. These include techniques such as pressure drop, residence time distribution and voltage loss.

Pressure drop

Pressure drop is a measurable parameter which can be used to quantify fuel cell flooding. This method is able to detect flooding as the presence of liquid water found either in the porous gas diffusion layer or in the flow field causes the gas flow resistance to rise. This in turn results in an increase in the pressure drop across the fuel cell. The pressure drop data needed for analysis is collected using pressure transducers which measure pressure drop across each half of the fuel cell.

Barbir et al. (2001) and He et al. (2003) were the first two studies which really highlighted the usefulness and reliability of this method of water detection. The studies observed the pressure drop in a fuel cell with interdigitated flow fields. The experimental tests which were conducted in these papers used a variety of operating conditions which were known to cause either flooding or drying of the fuel cell. Both studies reported that a pressure drop increase was experienced when there was liquid water accumulation in the fuel cell. Furthermore, they also reported that this measurement technique was a very reliable method for qualitatively assessing if there was flooding occurring within the system.

Another one of the major findings of these two studies was that no pressure drop was experienced when the fuel cell was experiencing conditions which caused cell drying. Barbir et al. (2001) therefore conducted further testing using cell resistance measurement to determine if the cell is drying. They reported that cell resistance readings increased when the fuel cell was drying and remained constant when the cell was flooding. This result showed that by using the pressure drop data in conjunction with the cell resistance data, one is able to determine if the fuel cell is flooding or experiencing cell drying.

There are however some shortfalls to this method of water detection. The first being that this method is unable to provide information regarding the liquid flow regimes present in the cell. This is particularly important when one is trying to improve fuel cell design. Another shortfall of this method is that it is unable to provide information as to where the water accumulation is taking place in the cell. This limits the ability to mitigate the problem of flooding in the cell.

Based on the initial findings by the studies conducted by Barbir et al. (2001) and He et al. (2003) General Motors developed both a method and apparatus for the detection and mitigation of

flooding in hydrogen fuel cells. The method and design was patented in 2002 (Barbir et al., 2005). The system was designed to monitor the pressure drops across both the anode and cathode flow fields and compare the readings to predetermined thresholds. If the pressure drop measured exceeds the predetermined threshold, corrective measures are automatically initiated. These corrective measurements include the turning-off of humidification systems and/or the reduction of gas pressure (Mathias and Grot, 2002).

In a different study by Hussaini & Wang (2009), pressure drop measurements across the cathode were used to determine the effect of water accumulation in a fuel cell. This studies shows the development of a mathematical coefficient which can be used to express the pressure drop over a two-phase region. This coefficient can be defined mathematically using Equation 6:

$$\phi_{2P} = \frac{\Delta P_{actual}}{\Delta P_{single\ phase}} \tag{6}$$

The actual pressure drop used in Equation 6 is the recorded measurement obtained from the pressure transducer during fuel cell operation. The assumption made in this study was that the actual pressure drop values included the effects of any liquid water present in the channels. The single phase pressure drop term used in Equation 6 was taken to be the mean measured pressure drop when operating with an open circuit. Before taking this measurement, the system was purged of all liquids. A calculated value of 1 for the coefficient implies that there is no liquid water in the system.

The reason for the development of this coefficient was to assist in the comparison of the degree of flooding between various tests. However, this coefficient has rarely been used in any subsequent literature available.

Residence time distribution

Resident time distribution (RTD) is another technique which can be used to detect and quantify the presence of liquid water in fuel cells during operation. This method makes use of tracer studies to determine the presence of liquid water in a fuel cell. This method is not commonly used in literature. The reason for this was that not many studies were able to find an accurate tracer/detection system combination which was minimally invasive.

One study which yielded positive results was conducted by Diep et al. (2007). In this study, they made use of a volume sensitive RTD technique to quantify the liquid water present in the flow fields and gas diffusion electrodes (GDE) of a fuel cell. In this study four different tracers and

detection system combinations were experimentally tested however the results were focused on the tracer/detection combination which yielded the best results. The combination focused on used a carbon dioxide tracer with an infrared detection system. The tracer was delivered to the system for both cases using the apparatus shown in Figure 10.

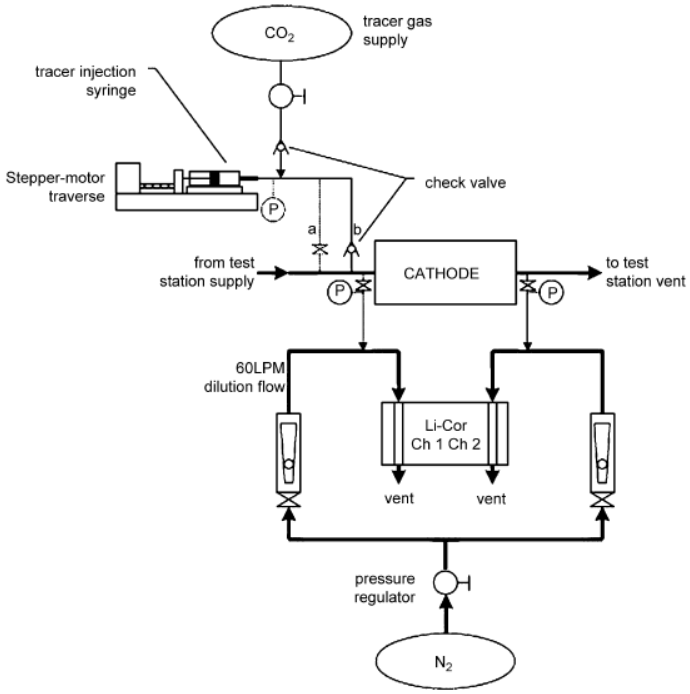

Figure 10: Schematic of the residence time distribution system used (Diep et al., 2007)

The detection system shown in Figure 10, used an infrared measurement system. This system was used to detect the amount of light absorbed within the test volume. The absorption measured on this system was done at a specific frequency within the spectrum and therefore, any observed change in the readings could only be due to the presence of carbon dioxide in the system.

The advantage of this method of water detection is that it is very sensitive to the changes in two phase flow of the system. Furthermore, it was able to produce results which were reproducible. The disadvantage of this method is that it has a high initial equipment cost. It also requires regular maintenance in order to achieve accurate results.

Voltage loss

When fuel cell flooding occurs, liquid water blocks some of the reactant transport pathways to the electrode surface. This causes a decrease in the cell voltage (Zhang et al., 2010). The impact of water accumulation in a fuel cell can therefore be measured in terms of the magnitude of the voltage drop experienced by the cell.

Hussaini & Wang (2009) conducted a study which considered the use of voltage loss as a water detection technique. Experiments were conducted by measuring the average voltage loss experienced over a 2-min interval following a period of 25 minutes of fuel cell operation. From the results obtained, the study reported that under conditions of extreme flooding the cell voltage measured was found to fluctuate erratically. This was determined to be due to formation of high-frequency water slugs in the gas channels of the fuel cell. Voltage losses as high as 80mV can be found during electrode and channel flooding. This is a major loss in performance of the fuel cell. This method was however not very sensitive in cases where the flooding was not as extreme.

2.5.3. Electrochemical techniques

The electrochemical techniques focus mainly on the resistance measurements in the cell. One example of this type of technique is EIS. EIS is advantageous as a water characterisation technique as it is capable of detecting in-situ changes in the PEFC with minimal disturbances of the system.

As mentioned in Section 2.4.2, EIS data can be displayed using both the Bode and Nyquist forms. In this particular study, Nyquist plots will be the only EIS plots used. The rest of this section will therefore be focused on this particular form of the EIS analysis. According to Yuan et al. (2010), a combination of electrical circuit elements can be used to model the impedance of a PEFC. These electrical elements may include but is not restricted to resistors and capacitors. Equivalent EIS circuits can be described as circuits where the electrical model that identically model the EIS response signal generated by the PEFC system. Since the various process in the fuel cell occur at various frequencies and/or time constants, each electrical element in the equivalent electrical circuit can be used to describe a specific process in the fuel cell (Yuan et al., 2010).

Figure 11 depicts the Nyquist plot along with the equivalent Randles circuit for a typical a simple fuel cell system. From Figure 11, the two distinct semicircles can be seen shows that the system being described has two time constants. In this case it is one for the anode side (smaller semi-circle) and one for the cathode side (larger semi-circle). The tail end of the graph takes a linear form indicating the Warburg impedance (Z_w), which describes the mass-transfer limitations within the fuel cell (Barbir, 2005). Fuel cell membrane saturation can be monitored by observing the impedance measurements carried out at high frequencies. This is depicted as the distance R_Ω in Figure 11. The charge transfer resistance of the system can be read off as the distance $R_{f,C}$ on the same figure.

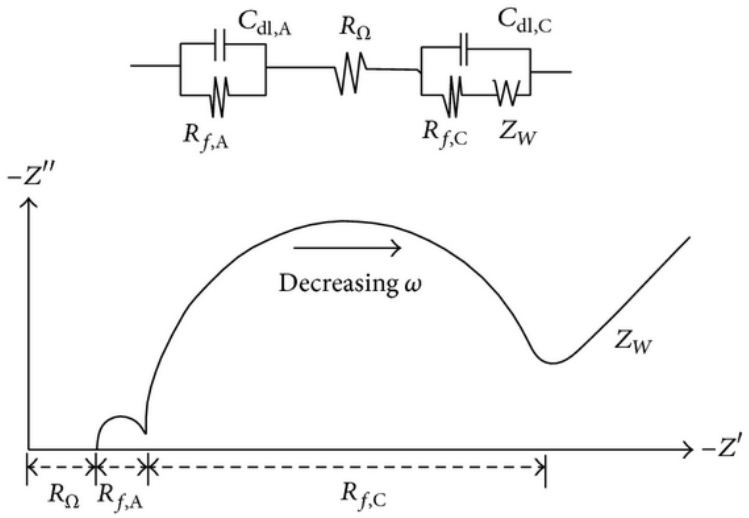

Figure 11: Typical Nyquist plot of a fuel cell with the equivalent Randles circuit (Chang et al., 2014)

Gebregergis et al. (2010) ran a study on PEMFC fault diagnosis, modelling and mitigation. In this study EIS measurements were successful used to isolate and quantify information regarding drying of the fuel cell membrane as well as fuel cell flooding. Figure 12 shows the Nyquist plots obtained in the study for fuel cell systems operating at normal, flooded and dried conditions.

Cha et al. (2006) conducted a study to determine if the microchannel (>100μm) flowfield design led to increased flooding. This study used the charge transfer resistance to determine if the cell was depicting signs of flooding. The results of the study showed an increase in charge transfer results for the microchannel system. This was attributed to an increase in flooding in the system. This study therefore showed that EIS could be used to determine the charge transfer resistances in a PEFC which employed a microchannel flowfield design.

Another study by Le Canut et al. (2006) completed a study which used EIS as a tool to detect membrane dying, fuel cell flooding and poisoning of the anode catalyst for a PEFC stack. From the study conducted, it was concluded that the EIS information was sufficient to draw conclusions based on membrane drying and fuel cell flooding.

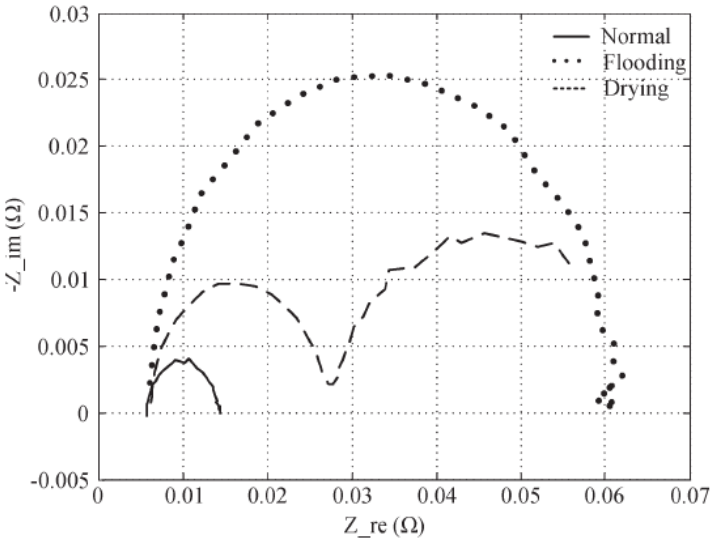

Figure 12: Nyquist plotting depicting fuel cell operation normal, flooded and dried conditions (Gebregergis et al., 2010)

3. Objective of study

Water management is a crucial aspect of PEFC operation which affects both its performance and durability. Improved water management is particularly critical for applications requiring high power density, such as automotive and aerospace applications.

Microchannel flowfield designs possess characteristics which can potentially improve water removal from the fuel cell and also reduce the fuel cell system complexity. There is limited knowledge on the use of microchannel flowfield designs in PEFCs, specifically how different operating conditions and different MEA designs affect the overall performance and water management of a fuel cell using microchannel flow fields.

One of the current water management strategies for PEFC's involves modifying the MEA structure, typically modifications to the carbon fiber based GDL. Whilst improvements have been observed, the current GDL designs still suffer from gas distribution and flooding problems. Metal based GDLs with uniform controlled structures have been proposed as a GDL alternative. The metal GDLs have consistently shown inferior performance to carbon based GDLs however very little work exists on modifying layers adjacent to the metal GDL, specifically the MPL that is typically coated onto a GDL.

The objectives of this study are therefore to:

- Investigate conventional methods of water removal, viz. manipulation of operating conditions in a single cell employing uniform structured metal GDLs and microchannel flowfields
- Determine the influence of modifying the wettability of the MPL on the performance of a single cell employing uniform structured metal GDLs and microchannel flowfields
- Compare the water management of a carbon paper GDL based system to a uniform structured metal GDL based system in a single cell employing microchannel flowfields.

Based on the literature analysed, the following hypotheses are proposed:

1. A single cell employing a microchannel flowfield design will show a similar trend to a single cell employing a conventional minichannel flowfield design when the cathode flowrate is increased viz. an increase in cathode flowrate will improve the water removal from the fuel cell due to an increased drag force.
2. A single cell employing uniform structured metal GDLs in combination with an MPL and microchannel flowfield design will show improved performance at high current densities in comparison to a system employing carbon GDLs. The metal based system leads to improved water removal due to a shorter water removal pathway.

3. Metal GDLs can be combined with MPLs of higher PTFE content than is typically used for carbon GDLs. The negative effect of the high PTFE content on ohmic resistances will be negated by the improved electronic contact of the metal GDL and microchannel flowfield system.

4. Experimental

This section describes the experimental methodology followed in this study. Information regarding the different experimental cases investigated is first presented. This is followed by a description of the procedure followed for the preparation of the MPLs used in the study. A detailed description of the single cell assembly setup is then provided and lastly the fuel cell diagnostic tools and testing procedures followed is presented.

4.1. Experimental cases

Four different experimental cases were investigated in this study. The cases varied in terms of the GDL and MPL designs used on the cathode side of a single fuel cell. All other components of the single cell were kept constant. The different cases were chosen based on their potential effect on the water management in the fuel cell. A summary of the different cases is presented in Table 1.

Table 1: Summary of the various cases investigated

Case	GDL material	GDL manufacturer	GDL thickness (µm)	GDL description	MPL PTFE content (wt%)
1	Carbon	Freudenberg Fuel Cell Component Technologies	210	• Carbon paper with 5wt% bulk hydrophobic treatment. • Product code: H2315 I6	20
2	Metal - stainless steel	Toyo Precision Parts MFG Co. Ltd	30	• Perforated metal sheet with hole diameter of 60 µm and pitch of 110 µm • Surface treated with 1 µm gold coating • No bulk hydrophobic treatment	15
3					20
4					30

4.2. Preparation and application of MPL

The ink used for the preparation of the MPL consisted of a conductive carbon powder additive (Cabot LITX200), de-ionised water, Triton™ X-114 (Sigma-Aldrich) and a 60wt% PTFE solution (Fuel Cell Earth Teflon Emulsion TE3859). Apart from the PTFE solution, the amount of each component was constant as is shown in Table 2. The PTFE amount varied depending on the final desired PTFE content in the MPL.

Table 2 shows the recipes used for the MPL inks fabricated for the various cathode GDL cases shown in Table 1.

Table 2: Recipes used for MPL fabrication for the various cases tested

Component	Mass (g)
Conductive carbon	3.00
De-ionised water	7.82
Triton X-114	5.32
PTFE solution	0.88, 1.25 or 2.14
Total	17.02

The components were all added to a beaker and hand stirred for 10 minutes. The resulting ink was then applied onto the GDL using the doctor blade coating technique. Prior to the coating the GDL thickness was measured using a Mitutoyo ABSOLUTE thickness gauge. A blade height of 100µm was used in order to achieve a dry MPL thickness of 30µm. The same mixing and application procedure was followed for all MPL coatings.

Following the coating, the GDLs were placed in a Memmert oven operating at 60°C for 1 hour. The GDLs were then placed in a Nabertherm furnace at 350°C for an hour. This was done to sinter the PTFE and remove the remaining deionised water and triton from the MPL. Once the coated GDLs were cooled and removed from the furnace, the thickness was measured using the Mitutoyo ABSOLUTE thickness gauge.

4.3. Fuel Cell Assembly

In-situ testing of the different experimental cases were conducted in a single fuel cell environment.

4.3.1. Description of single cell components

A description of the various single cell components used in this study is presented in Table 3. Apart from the cathode GDLs, all the components used were obtained from commercial suppliers. Figure 13 presents pictures of the assembled single cell and a flowfield plate.

Table 3: Description of single cell components

Component Name	Manufacturer	Description
End plates	Pragma Industries	• Aluminium material with external anode and cathode heating cartridges • Holes machined for 8 tie rods and bolts
Catalyst coated membrane (CCM)	Ion Power	• Product code: MEA-XL • Nafion® XL membrane • Active area: 25cm^2 • Equivalent anode and cathode platinum catalyst loadings of 0.3mg·cm^{-2}
Anode GDL	Freudenberg Fuel Cell Component Technologies	• Product code: H2315 I3 C1 • Carbon paper with MPL • Thickness: 260µm • Bulk PTFE loading: 10wt%
Anode and cathode flowfield plates	Toyo Precision Parts MFG Co. Ltd	• Gold plated stainless steel plates • Straight microchannel flow field pattern • Channel width: 0.2mm • Channel depth: 0.1mm • Rib width: 0.1mm • No hydrophobic treatment
Anode and cathode current collector plates	Pragma Industries	• Gold plated stainless steel plates • Gas entry/exit holes lined with rubber o-rings
Insulation sheet	Quadrant engineering plastics	• PTFE coated fibre glass • Thickness: 75 µm
Anode gasket	Sanshin Enterprises Co. Ltd	• Silicone material • Thickness: 200 µm
Cathode gasket for carbon GDL cases	Sanshin Enterprises Co. Ltd	• Silicone material • Thickness: 200 µm
Cathode gasket for metal GDL cases	TERAOKA SEISAKUSHO Co., Ltd	• Product code: 635F PEN Tape • PEN film with an adhesive • Thickness: 40 µm

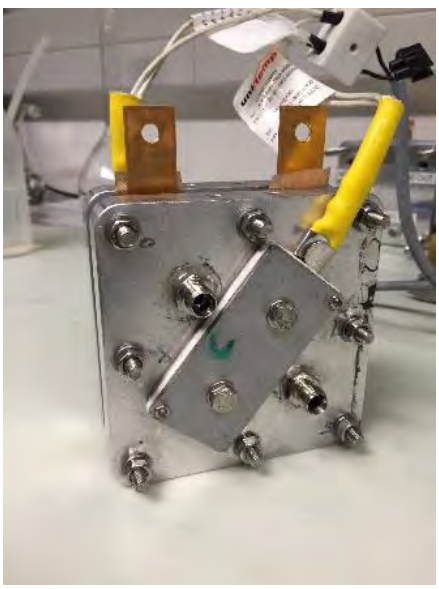

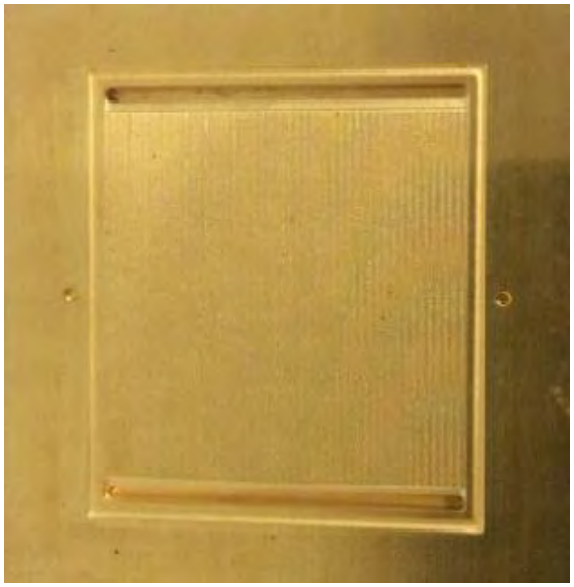

Figure 13: Assembled single cell fixture and flowfield plate

4.3.2. Assembly procedure

Before the fuel cell was assembled, the current collector plates and flowfield plates were wiped using Isopropanol and lint free tissue. This was done to remove any foreign particulate materials from the plates which might influence the fuel cell performance.

For all tests a new set of catalyst coated membrane, anode and cathode GDLs and gaskets were used. The same set of end plates, flowfield plates, current collector plates and insulation sheets were used for all tests in the study.

The end plates had holes for 8 tie rods. All cell components were placed in between the end plates and compressed using a torque wrench. A cell torque of 1.4Nm was applied on all 8 bolts. The tools used and the torqueing procedure is shown in Figure 14A. A cell torque of 1.4Nm on the 8 bolt system where the bolt diameter was 5mm translates to a cell compression pressure of 1.8MPa.

The torqueing of the cell was done in increments of 0.2Nm in the order shown in Figure 14B. The process was conducted in this prescribed pattern to maintain even compression across the cell and minimize damage to internal cell components.

A

B

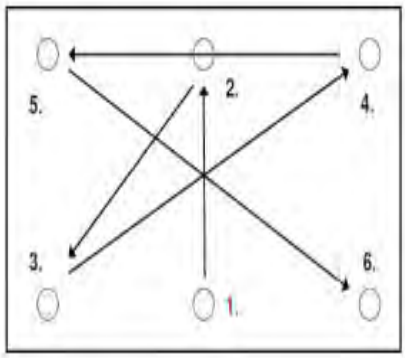

Figure 14: (A) Tools used to compress the cell (B) Tightening pattern at each torque setting

4.4. Fuel cell testing

All the single cell tests were performed using a FuelCon test station (Evaluator C50-LT). The FuelCon test station consisted of the following main components: an electronic mass flow controller, anode and cathode external humidification systems, heated and insulated gas inlet lines, temperature control systems, backpressure regulators, electronic load (TrueData-LOAD®) and a computerized system for data collection. During the fuel cell operation, the system settings were monitored and controlled using the data acquisition system connected to a computer using the FuelWork® software. The fuel cell heating, conditioning and diagnostic tests were all run using automated testing scripts which were developed in-house.

Pure hydrogen gas (supplied by Air Liquide with a purity of 99.999%) was used as the anode reactant gas for all diagnostic tests conducted for this study. This gas was supplied to the system using a pressurised gas cylinder. Both air and oxygen were used as oxidant reactant gases for the various tests conducted. Air was supplied to the system using an Atlas Copco air compressor. The pure oxygen (purity of 99.999%) was attained from a pressurised gas cylinder. The pure nitrogen (supplied by Air Liquide with a purity of 99.999%) used for some of the pre-diagnostic procedures was also supplied to the system by a pressurised gas cylinder.

4.4.1. Fuel cell start-up procedure

Once the cell was assembled and compressed, the cell was placed on the test station and the cell heating cartridges were connected. The temperature probe was inserted in the designated hole in the cathode flow field plate. Sense cables which are responsible for measuring the impedance and cell voltage across the cell were inserted into anode and cathode flowfield plates. The anode and cathode load connecting cables were then attached to the respective current collector plates. Lastly, the anode and cathode inlet and exhaust lines were connected. Special care was taken to ensure that the all the connection points between the cell and gas lines were properly sealed to prevent any gas leakage.

Once the cell was connected to the fuel cell test station, a leak test was performed on both the anode and cathode compartments. This test was conducted to verify if the cell was adequately sealed. The first step of this procedure required the anode and cathode exhausts to be closed. Both compartments were then pressurised to 1.35 bar using nitrogen gas flowing at a rate of 25Nl/min. Once the target pressure was reached, the inlet gas flow was stopped and the cell pressure was observed for a period of 5 minutes. If the pressure drop observed over this time period was found to be less than 0.05 bar, the single cell was deemed appropriately sealed and the cell heating and conditioning was commenced. If the pressure drop was found to be greater than 0.05 bar, the cell was disassembled, the individual components were realigned and the fuel cell assembly and start-up procedures were repeated.

Once the cell was deemed to be sealed, the heating of the cell, gas inlet lines and humidifiers were carried out. The heating procedure was done incrementally until the operating set point temperatures were reached. During this procedure nitrogen gas was passed through the cell at a flow rate of 25Nl/min.

Before the fuel cell diagnostic tests were commenced, the membrane and catalyst layers were humidified. This was achieved by operating the fuel cell at the set conditions shown in Table 4. During this procedure, the cell voltage was cycled between 0.3V and 0.8V for ten cycles. Each cycle began with a 30 second wait at 0.8V. This was followed by a 10 minute wait period at 0.3V. At the end of each cycle a high frequency resistance (HFR) measurement at 10 kHz was recorded. The HFR reading after each cycle helped to monitor the ohmic resistance experienced by the cell. This provided insight on the hydration of the membrane of the cell.

Table 4: Operating conditions used for fuel cell conditioning cycles

Anode gas	Hydrogen
Cathode gas	Air
Anode gas flow rate (Nl/min)	0.64
Cathode gas flow rate (Nl/min)	2.49
Cell temperature (°C)	80
Anode relative humidity (%)	100
Cathode relative humidity (%)	100
Anode/Cathode backpressure (bar)	1

4.4.2. Diagnostic tests

Overview of fuel cell tests and operating conditions

Table 5 summarises the different tests and operating conditions used in this study. Most of the tests were conducted at constant anode and cathode flowrates, corresponding to stoichiometric flows at a current density of 1.5 A·cm^{-2}. Tests 6-8 were conducted using stoichiometric or load following flowrates. This implies that the flowrates were altered based on the current being drawn and at a certain stoichiometric ratio.

Table 5: Summary of tests and operating conditions

Test No.	Experimental case (Table 1)	Operating conditions						Diagnostic tests performed
		T (°C)	P (bar)	RH (%)	S_{anode}	$S_{cathode}$	Cf/Lf	
1	1	80	1	100	1.5 at 1.5 A·cm^{-2}	2, 2.5, 3, 4 at 1.5 A·cm^{-2}	Cf	• Polarisation curves • EIS
2	2							
3	3							
4	4							
5	1				1.5	2, 2.5, 3, 4	Lf	• Two phase pressure drop coefficient tests • Voltage stability tests
6	2							
7	3							
8	4							
9	1		a = 1, c = varying*		1.5	2	varying *	• Polarisation curves

Cf = Constant flow, Lf= Load following
**Procedure described in Section 4.4.2 - cathode stoichiometry investigation*

Polarisation curves

Polarisation curve measurements were carried out in galvanostatic mode. Prior to the measurement the relevant operating flowrates were set. The fuel cell was set to OCV conditions and a stabilization period of 3 minutes was allowed. After this period, three readings were recorded with a wait period of 10 seconds between each reading. From the three voltage readings an average was calculated and this value was used to generate the polarisation curve plot. After the third voltage reading, an HFR measurement was conducted at a frequency of 10 kHz.

Following the OCV measurement the current was increased incrementally and voltage and HFR measurements were repeated as described above. The current was increased in increments of 0.5 A in the activation region and 2 A for the rest of the curve. This was continued until either the maximum current or minimum voltage was reached. The maximum current and minimum voltage was set at 50 A and 0.3 V respectively. These maximum current and minimum voltage values were set to avoid degradation or damage to fuel cell components.

EIS

Immediately after the polarisation curve tests were performed, EIS measurements were conducted at 0.25 $A \cdot cm^{-2}$ and 1.2 $A \cdot cm^{-2}$. This was done for Tests 1-4. To allow for sufficient settling time at a new set of conditions, a wait period of 30 minutes was employed prior to each test.

The EIS measurements were carried out by introducing a sinusoidal current, of a known amplitude, to the system being tested. The amplitudes used were in the frequency range of 0.1Hz -20 000Hz, using 8 steps in a decade. The amplitude of the responding current wave was then analysed.

Two-phase pressure drop coefficient test

Two-phase pressure drop coefficient tests were conducted for tests numbers 5-8. The relevance of the two phase pressure drop coefficient is described previously in Section 2.5.2 and is determined by measuring the pressure drop across the cathode compartment of the fuel cell under various operating conditions.

The pressure drop at the cathode side of the fuel cell at OCV was first measured by the use of pressure gauges at the cathode inlet and outlet. Following 5 minutes at OCV the pressure drop was recorded every 10 seconds over a period of 3 minutes at a specific cathode flow rate. The time preceding the measurement was limited to 5 minutes to prevent known long term effects of exposure to OCV. Following the OCV measurement the cell was set to operate at a certain current density. After a 25 minute waiting period the pressure drop across the cathode side of the fuel cell was then measured every 10 seconds over a period of 5 minutes. The aforementioned OCV measurements and current density measurements were for four different current densities of 0.25$A \cdot cm^2$, 0.5 $A \cdot cm^2$, 0.75 $A \cdot cm^2$ and 1 $A \cdot cm^2$ and for cathode stoichiometries of 2, 2.5, 3 ad 4.

Between each pair of readings (OCV and at a specific current density), the fuel cell was operated at a current density of 0.25$A \cdot cm^2$ while passing very high gas flow rates through the cell. The flow rates used corresponded to stoichiometries of 1.5 and 2 at 2 $A \cdot cm^2$ for the anode and cathode respectively. This was done for a period of 15 minutes to remove any residual water in the channels that would influence the results of the subsequent tests.

Voltage stability tests

Voltage stability tests were conducted for tests 5-8 immediately following the pressure drop co-efficient tests. Before the voltage stability tests were commenced, the fuel cell was operated at a current density of 0.25 $A \cdot cm^2$ for 15 minutes while passing very high gas flow rates through the cell. The flow rates used corresponded to stoichiometries of 1.5 and 2 at 2 $A \cdot cm^2$ for the anode and cathode

respectively. Similar to the reasons stated previously, this was done to remove any residual water in the channels of the flowfield that would influence the results of the voltage stability tests.

The voltage stability test consisted of operating the fuel cell at a particular current density and stoichiometry and monitoring the fuel cell voltage over a 2 hour period. The tests were conducted at current densities of 0.25 $A \cdot cm^2$, 0.5 $A \cdot cm^2$ and 1 $A \cdot cm^2$ and cathode stoichiometries of 2, 2.5, 3 and 4. The cell voltage was recorded every second over the two hour period.

Cathode stoichiometry investigation

Section 2.3.1 - Increasing flowrate, discussed the positive influence on fuel cell performance of increasing the cathode stoichiometry. Test 9 was carried out to help discern whether the increase in performance as cathode stoichiometry increases is mainly due to an increase in oxygen partial pressure or an increase in the drag force available to eject excess water from the cell. To do this, the cathode backpressure was adjusted at a constant stoichiometry of 2. Adjusting the back pressure ensured that the same oxygen partial pressure is maintained as would be present for a stoichiometry of 4 but the drag force would still be the same since the stoichiometry was still 2. This allows for the separation of the two effects experienced when increasing stoichiometry. Table 6 shows a summary of the average partial pressures of oxygen and exit pressures used at each current density.

Table 6: Summary of the average partial pressures of oxygen and exit pressures used for Test 9

Current Density (A)	Average Partial Pressure of Oxygen (bar)	Cathode Exit Pressure (bar)
0.02	0.162	1.11
0.04	0.162	1.11
0.06	0.162	1.11
0.08	0.161	1.11
0.16	0.161	1.12
0.24	0.160	1.12
0.32	0.160	1.13
0.40	0.159	1.13
0.48	0.159	1.14
0.56	0.158	1.14
0.64	0.157	1.15
0.72	0.157	1.15
0.80	0.156	1.16
0.88	0.155	1.16
0.96	0.155	1.17
1.04	0.154	1.18
1.12	0.154	1.18
1.20	0.153	1.19

1.28	0.152	1.20
1.36	0.152	1.21
1.44	0.151	1.21
1.52	0.150	1.22
1.60	0.150	1.23

5. Results and Discussion

This section presents the major findings of the study and a discussion of these findings. The results of the manipulation of operating conditions, specifically the varying of cathode stoichiometry, on a fuel cell employing conventional MEA components is presented first. This is followed by the results of changing the MEA structure, firstly the use of the metal based GDL and secondly the varying PTFE content in the MPL of the metal GDL system. It is important to note that the results of this study were specifically made for PEFCs using metal flowfield plates with a straight parallel microchannel channel design. All comparisons are presented and discussed with specific reference to water management within the fuel cell. A fold out page of the different GDL cases and test runs as presented in Tables A1 and A2 is available in Appendix 1 for the ease of the reader.

5.1. Manipulation of operating conditions: effect of varying cathode flowrate

Figure 15 shows the results obtained for Test 1, more specifically the effect of varying the cathode flowrate on the overall fuel cell performance of a carbon GDL based system. The polarisation curves show that an increase in the cathode flowrate improves the fuel cell performance at medium to high current densities. Negligible difference in performance is observed at low to medium current densities. This result is in accordance with trends observed in previous studies of similar systems (Zhang et al., 2010).

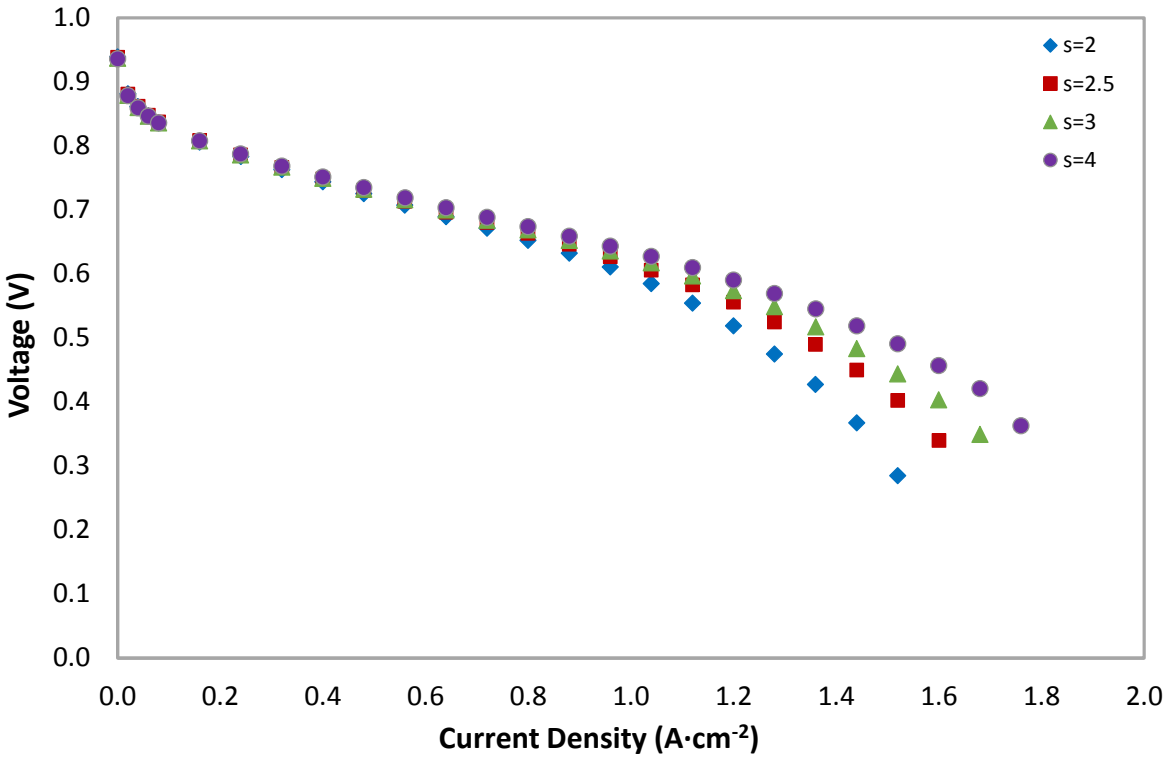

Figure 15: Effect of varying cathode flowrate on polarisation curve performance for a carbon GDL system (Test 1)

The significant differences in performance in the high current density region indicates that the different cathode flowrates influence the extent of mass transfer limitations being experienced within cathode compartment of the fuel cell. An increase in the cathode flowrate or cathode stoichiometric ratio not only increases the partial pressure of oxygen but also provides additional drag force which can be used to expel any accumulated liquid water within the system, particularly within the GDL and flowfields. The results observed in Figure 15 are attributed to a combination of the aforementioned factors.

Figure 16 shows the results for Test 9 which as previously explained was carried out to determine which of the two factors (increase in oxygen partial pressure or increase in drag force) is more dominating in terms of the results observed in Figure 15. Figure 16 shows the polarisation curves obtained for two different cathode flowrates (corresponding to stoichiometric ratios of 2 and 4 at 1.5 $A \cdot cm^{-2}$) and a cathode back pressure of 1 bar compared to a polarisation curve obtained when operating the fuel cell at the lower cathode flowrate (corresponding to a stoichiometric ratio of 2 at 1.5 $A \cdot cm^{-2}$) but with varying cathode back pressure. The latter conditions keeps the drag force constant

whilst varying the oxygen partial pressure to match the oxygen partial pressure experienced at the higher cathode flowrate.

Figure 16 indicates that an increase in the oxygen partial pressure significantly improves cell performance at the higher current densities. However, it does not achieve the performance obtained at the higher cathode flowrate. The additional improvement in performance is therefore the influence of the increased drag force experienced at higher cathode flowrates. The results indicate that for the carbon GDL system both factors are arguably equally influential and also confirms as expected that increasing the cathode flowrate is a viable water management strategy as it assists with the removal of liquid water.

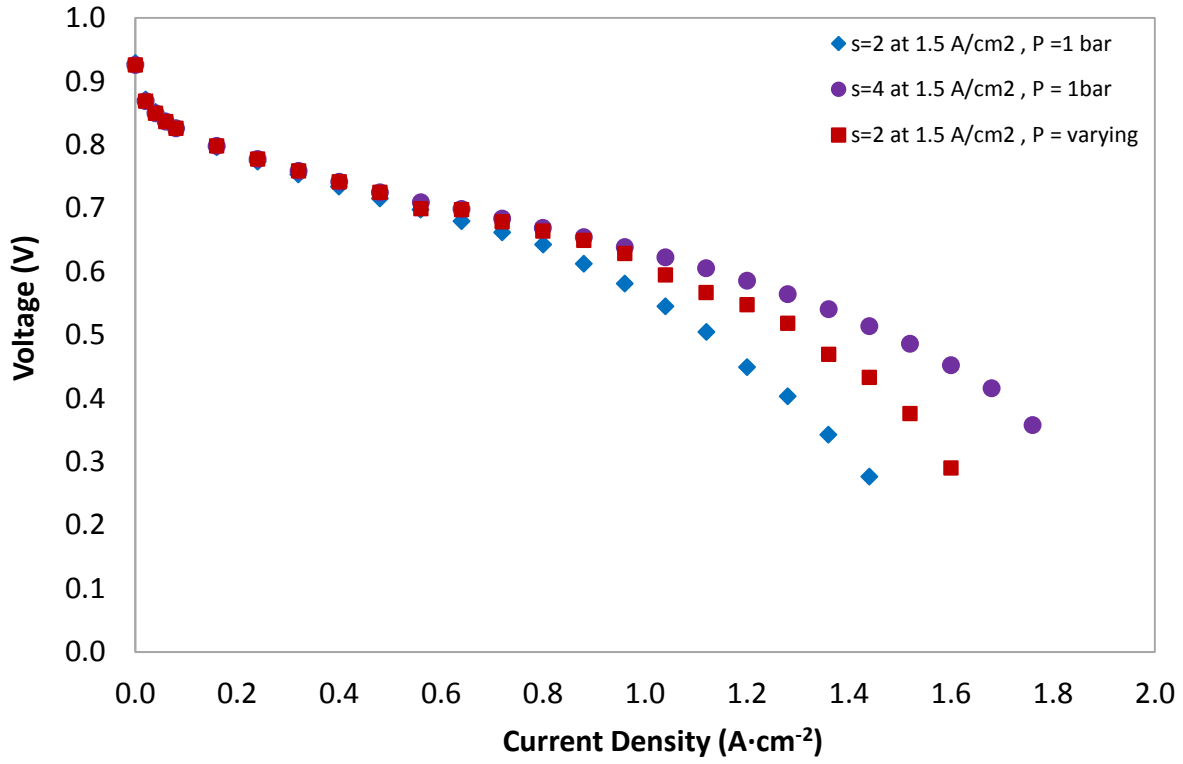

Figure 16: Effect of varying cathode back pressure at a constant cathode flowrate for the carbon GDL system. The result for a higher cathode flowrate is superimposed to discern the influence of increased oxygen partial pressure and increased drag force (Test 9)

5.2. MEA Materials and structure design: Metal GDL

The effect of varying the cathode flowrate for the different metal GDL and MPL cases on overall fuel cell performance is first presented followed by a comparison to the carbon GDL system. The results of the electrochemical impedance spectroscopy measurements is then presented for all cases to better understand the effect of the different MEA component designs. Finally the results of the

pressure drop co-efficient and voltage stability tests are presented to understand the influence of the different MEA component designs on water management.

5.2.1. Effect of varying cathode flowrate for metal GDL cases

Figures 17, 18 and 19 shows the effect of varying the cathode flowrate for the different metal GDL and MPL cases. Similar trends to a carbon GDL system are observed for all cases, viz. negligible difference in performance at low current densities and significantly improved performance at high cathode flowrates at high current densities. For the metal GDL case with an MPL of 20 wt% (Figure 18) the performance difference starts occurring at significantly lower current densities than the other cases.

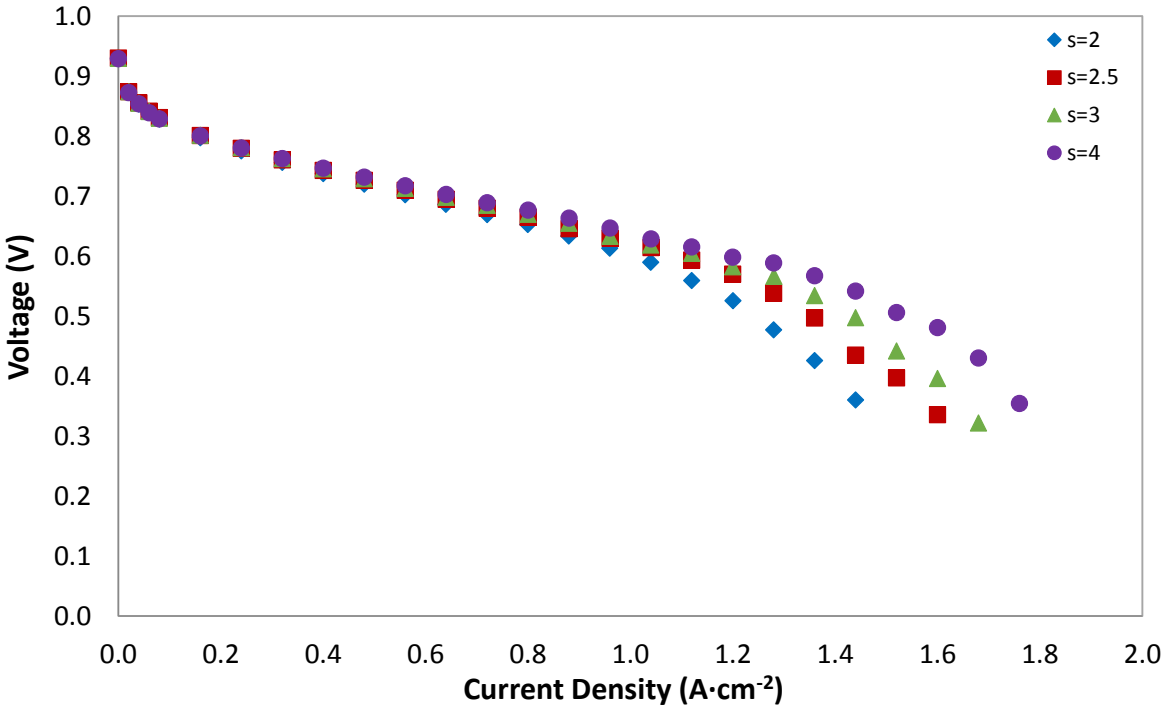

Figure 17: Effect of varying cathode flowrate on polarisation curve performance for a metal GDL with an MPL containing 15 wt% PTFE (Test 3)

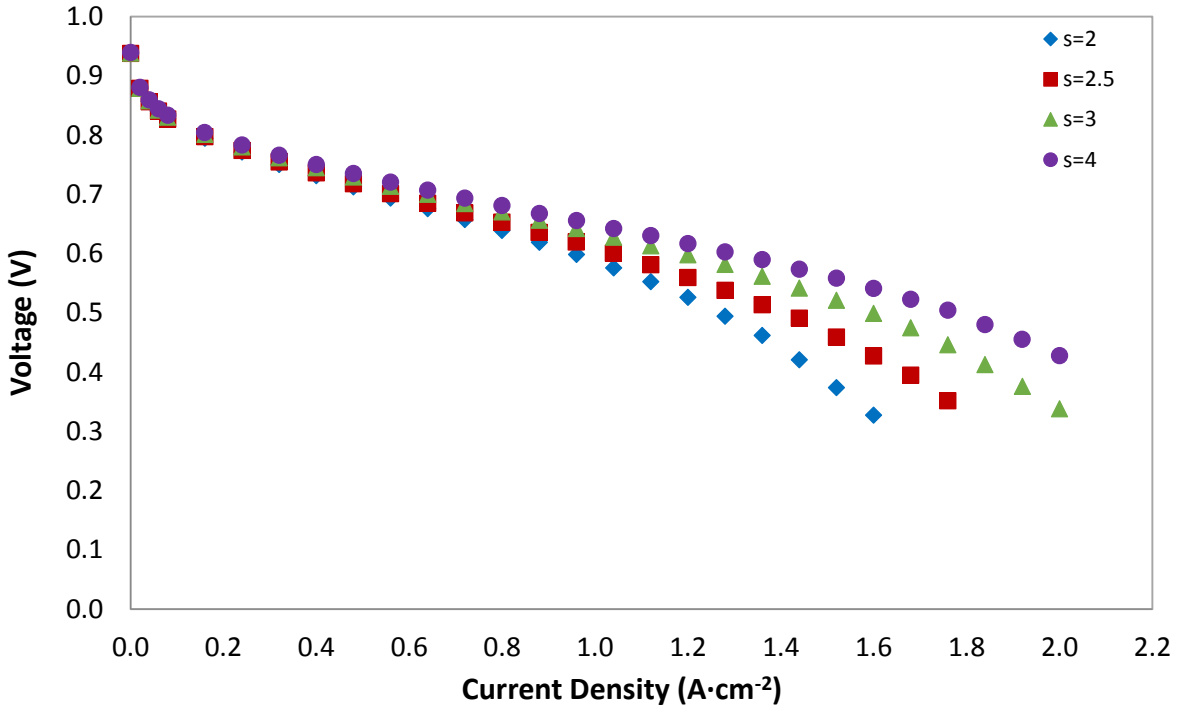

Figure 18: Effect of varying cathode flowrate on polarisation curve performance for a metal GDL with an MPL containing 20 wt% PTFE (Test 4)

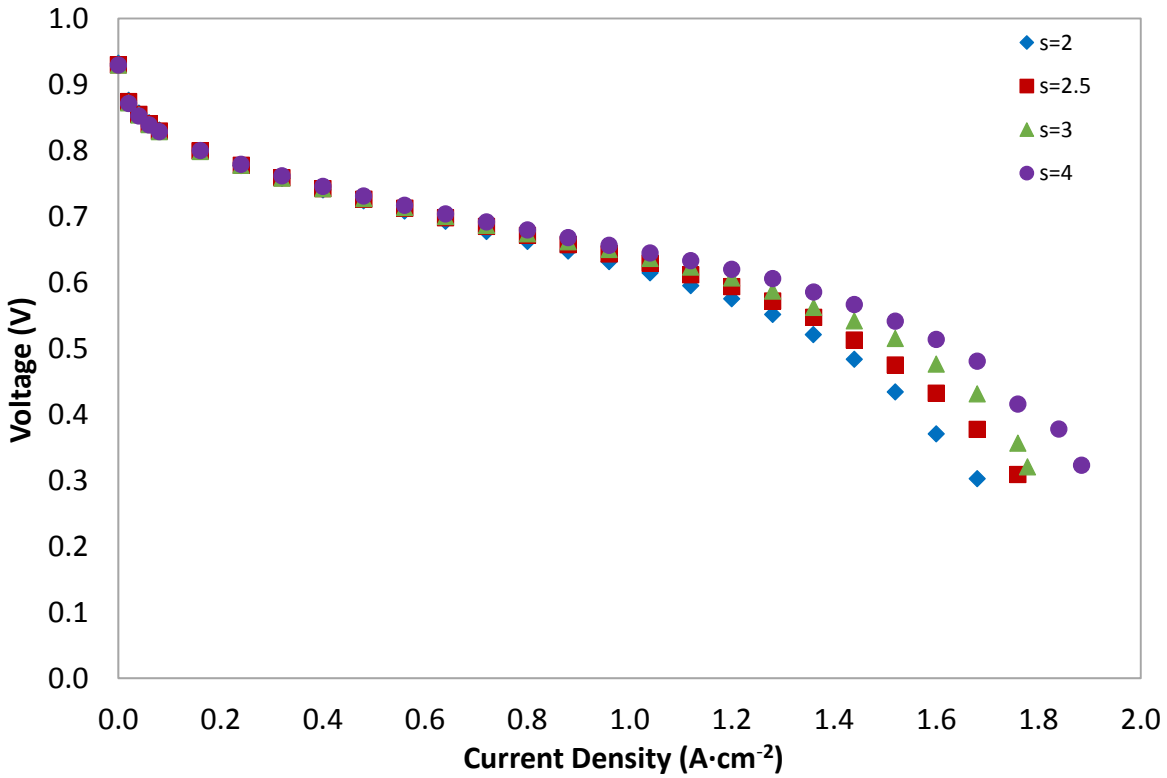

Figure 19: Effect of varying cathode flowrate on polarisation curve performance for a metal GDL with an MPL containing 30 wt% PTFE (Test 5)

From figures 15, 17, 18 and 19 the mass transfer limiting current can be obtained. Limiting current is typically described as the point where the cell voltage experiences a sudden drop due to insufficient

supply of reactant gases. This is observed as a near vertical drop and is indicative of severe mass transfer limitations. These losses are usually as a result of severe cell flooding and therefore the limiting current gives an indication of water build-up within the cell. Figure 20 shows the limiting current at each cathode flowrate for the all the GDL cases. It should be noted that the limiting current values were calculated from the as presented polarisation curves and not internal resistance (IR) corrected curves as is typically done. This is due to limitations on the fuel cell test station side, specifically the inability to measure the high frequency resistance in parallel with the polarisation curve measurement.

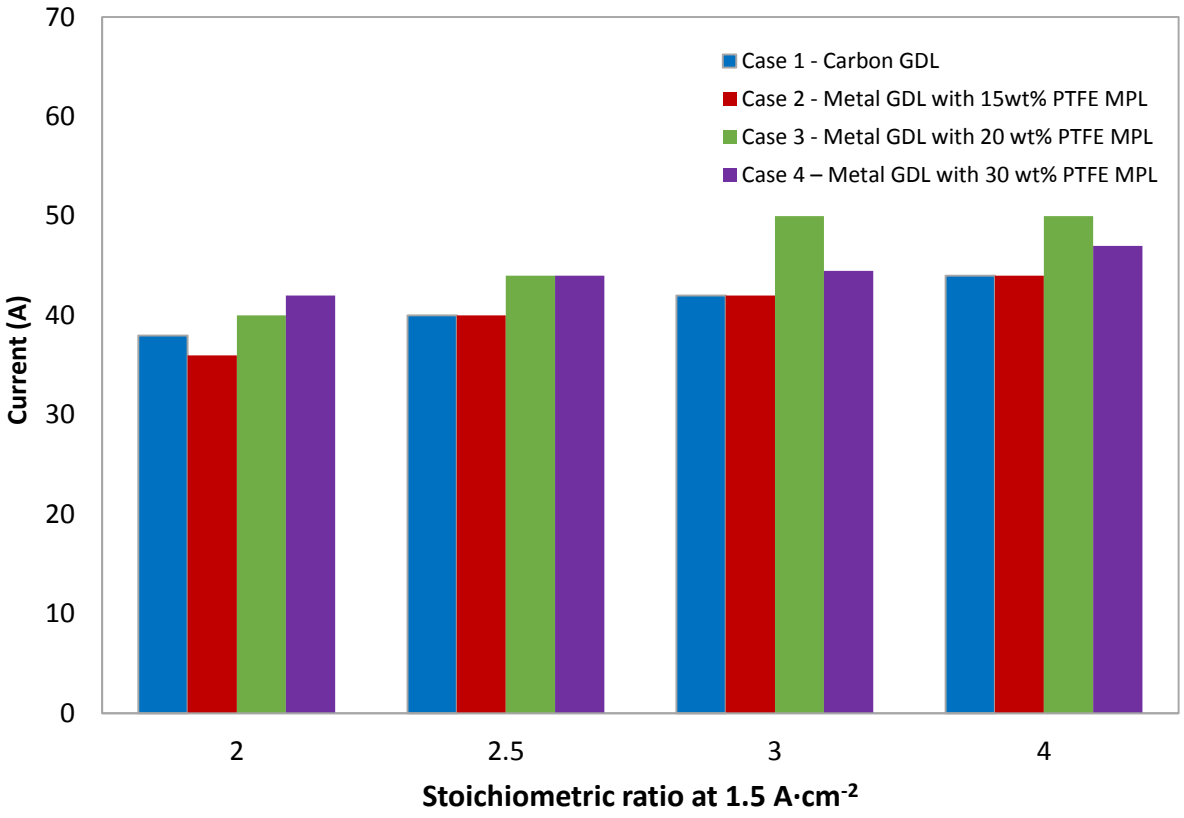

Figure 20: Comparison of limiting currents for the different MEA component designs at varying cathode flowrates

Figure 20 shows that highest limiting currents at all cathode flowrates were observed for the metal GDLs with MPL content of 20 wt% and 30 wt%. The result implies that the metal GDL with an MPL reduces the flooding within the fuel cell in comparison to the carbon GDL system. The higher PTFE content in the MPL appears to be required to assist with the water removal however too high a PTFE content may lead to resistance to gas flow due to less porosity. This explains the best results being observed for the metal GDL with 20wt% PTFE. The sensitivity of the metal GDL limiting currents with respect to changes in cathode flowrate is similar to that of the carbon GDL system. Overall the metal

GDL with MPL appears to be a good strategy for water management under the operating conditions used in this study.

5.2.2. Electrochemical Impedance Spectroscopy

Figures 21-24 show the Nyquist plots for all GDL cases for the EIS measurements conducted at 0.25 $A \cdot cm^{-2}$. By modelling the fuel cell as an equivalent Randles circuit, the ohmic and charge transfer resistances were estimated from the Nyquist plot and are presented in Figures 25 and 26 respectively.

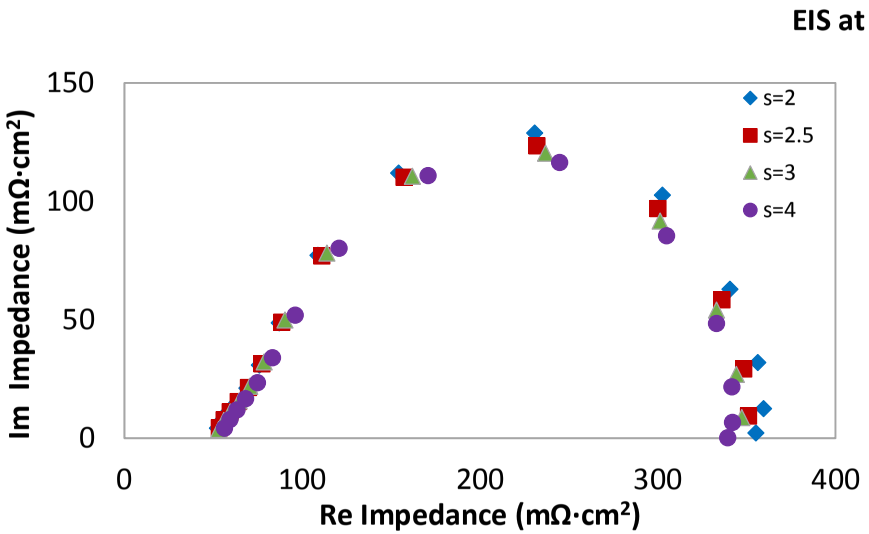

Figure 21: Nyquist Plot for carbon GDL at 0.25 A·cm^{-2}

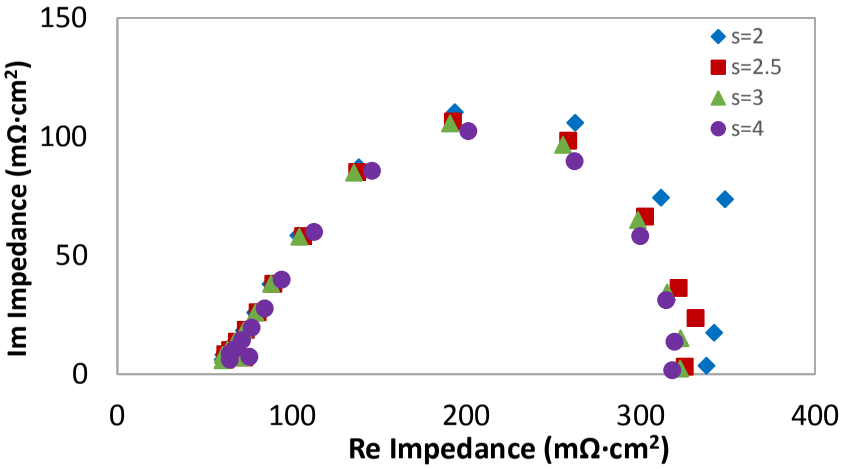

Figure 22: Nyquist Plot for Metal GDL with 15wt% PTFE MPL at 0.25 A·cm^{-2}

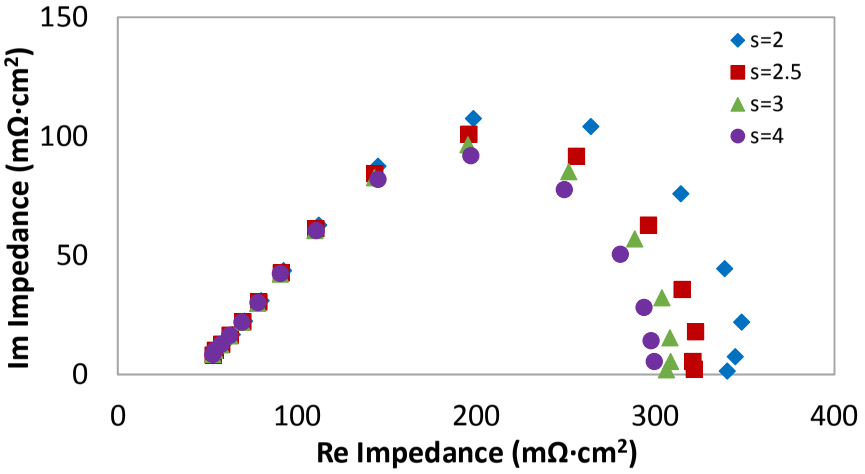

Figure 23: Nyquist Plot for Metal GDL with 20wt% PTFE MPL 3 at 0.25 A·cm^{-2}

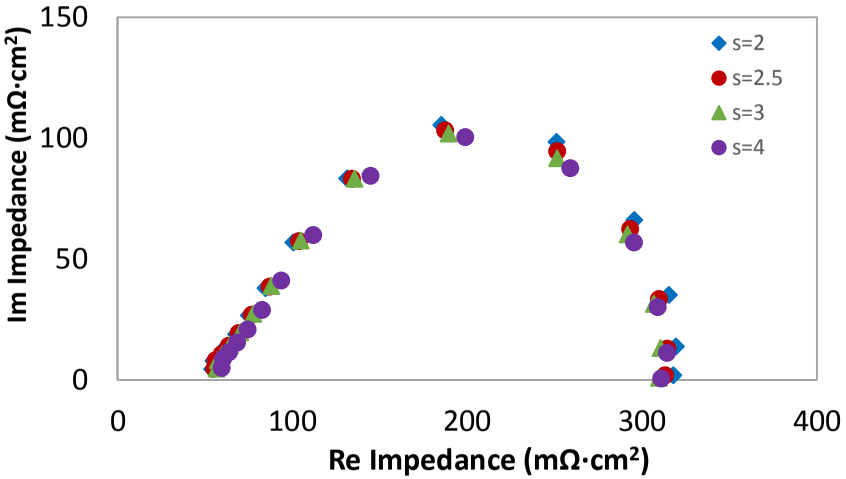

Figure 24: Nyquist Plot for Metal GDL with 30 wt% PTFE MPL at 0.25 A·cm^{-2}

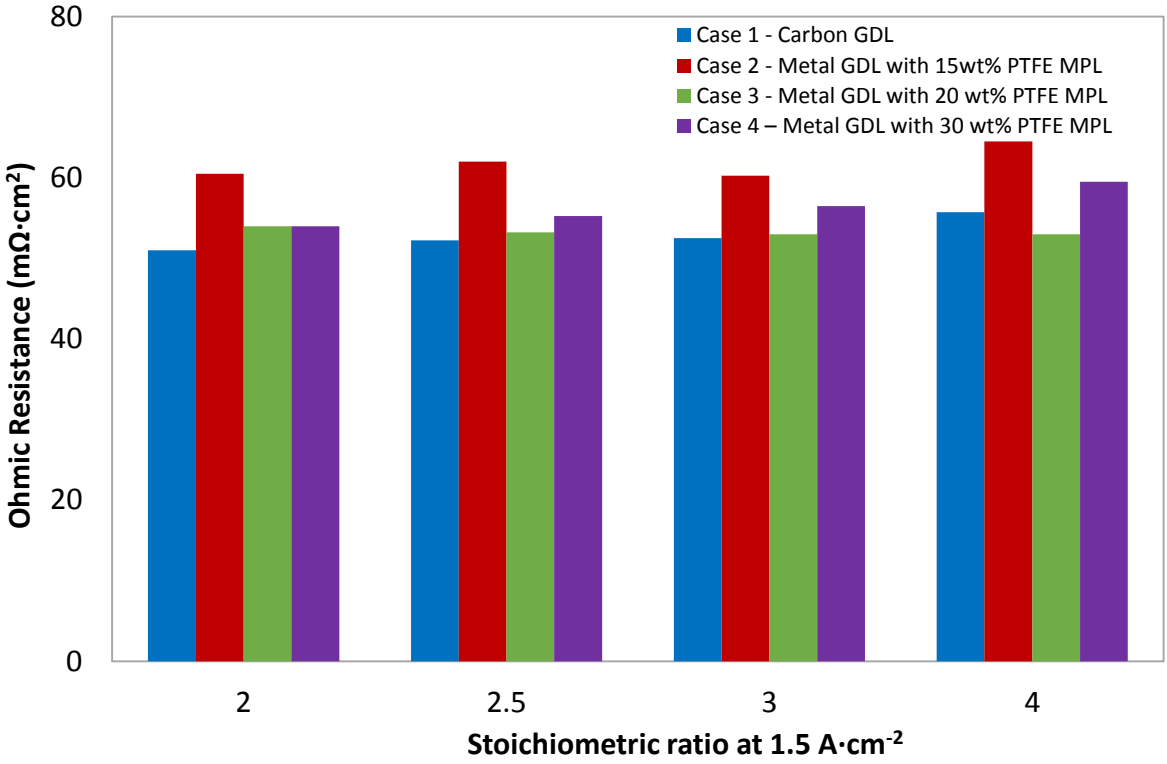

Figure 25: Comparison of ohmic resistances for all cases as a function of cathode flowrate at 0.25 A·cm^{-2}

Figure 25 shows a negligible change in ohmic resistance as cathode flowrate changes for all the GDL cases. Since the ohmic resistance is a strong function of the membrane resistance, this implies that the changing flowrate has minimal effect on the membrane saturation at a current density of 0.25 A·cm^{-2}. Figure 25 also shows that besides the metal GDL with 15wt% PTFE content in the MPL, the ohmic resistances were very similar across the different cases. The highest ohmic resistances for the 15wt% MPL is somewhat surprising since one would expect that a lower PTFE content in the MPL means better contact between the MPL and catalyst layer.

Figure 26 shows the highest charge transfer resistances were observed for the carbon GDL system for all cathode flowrates. Since the catalyst layer is the same for all cases, this implies that even at this relatively low current density the metal GDLs allow for improved mass transfer of reactant gases. The charge transfer resistances for the metal GDL systems are very similar. Overall, the minimal change in the ohmic and charge transfer resistances for all cases at 0.25 A·cm^{-2} as the cathode flowrate changes is in agreement with the polarisation curve results were negligible difference in performance is observed at different cathode flowrates.

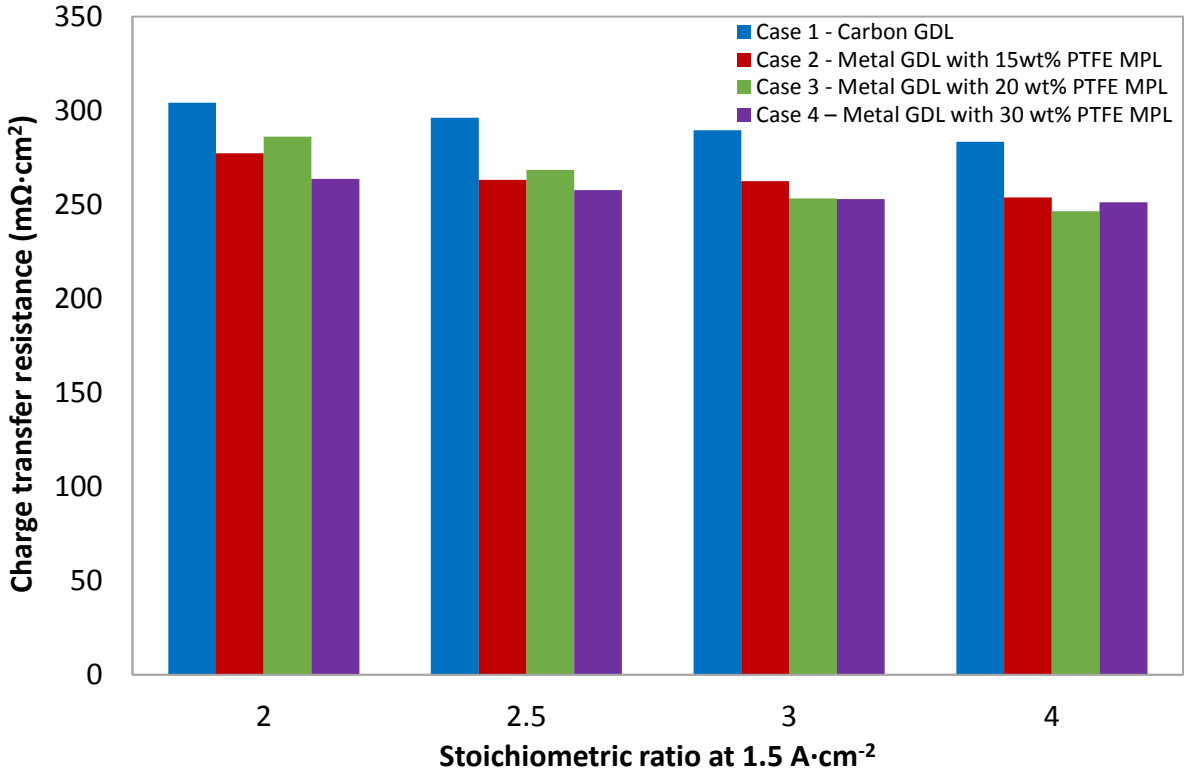

Figure 26: Comparison of charge transfer resistances for all cases as a function of cathode flowrate at 0.25 A·cm^{-2}

Figures 27-30 shows the Nyquist plots for all GDL cases for the EIS measurements conducted at 1.2A·cm^{-2}. Once again by modelling the fuel cell as an equivalent Randles circuit, the ohmic and charge transfer resistances were estimated from the Nyquist plot and are presented in Figures 31 and 32 respectively.

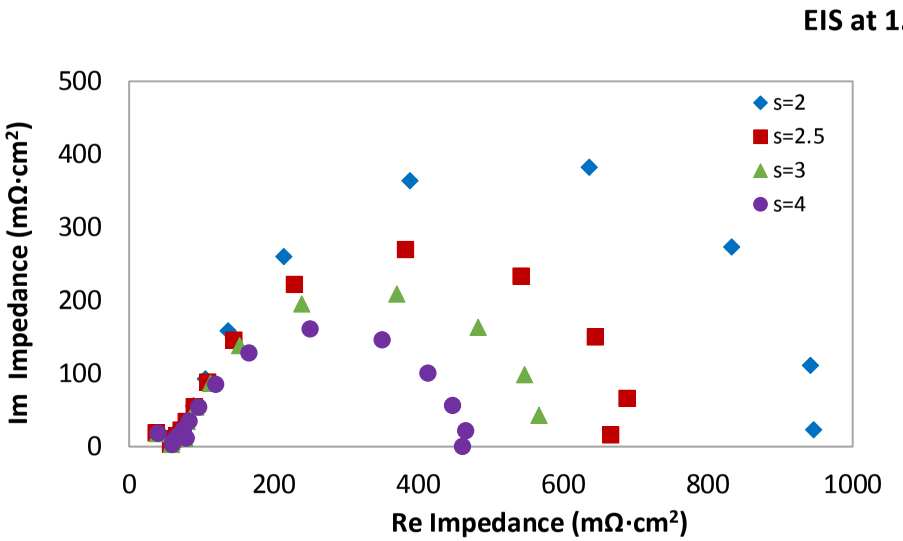

Figure 27: Nyquist Plot for carbon GDL at 1.2 A·cm^{-2}

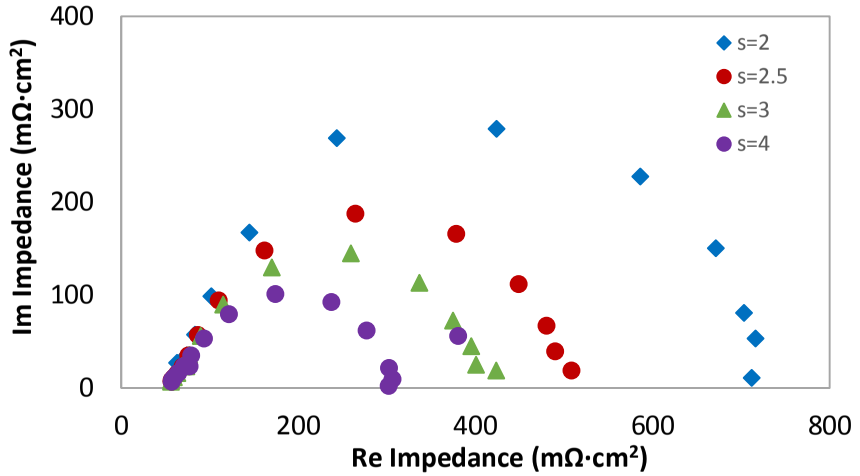

Figure 28: Nyquist Plot for Metal GDL with 15wt% PTFE MPL at 1.2 A·cm^{-2}

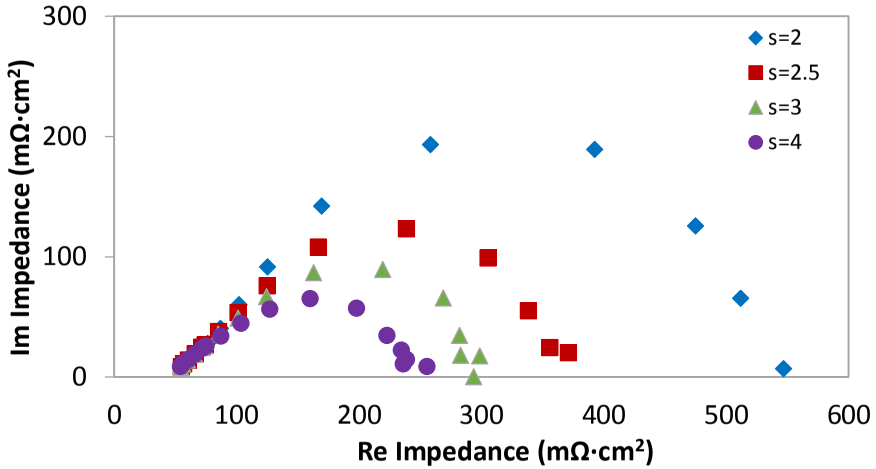

Figure 29: Nyquist Plot for Metal GDL with 20wt% PTFE MPL 3 at 1.2 A·cm^{-2}

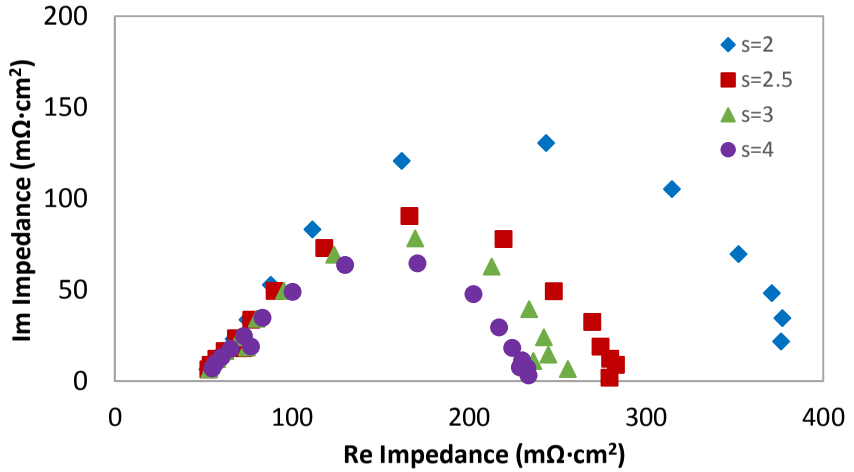

Figure 30: Nyquist Plot for Metal GDL with 20wt% PTFE MPL 3 at 1.2 A·cm^{-2}

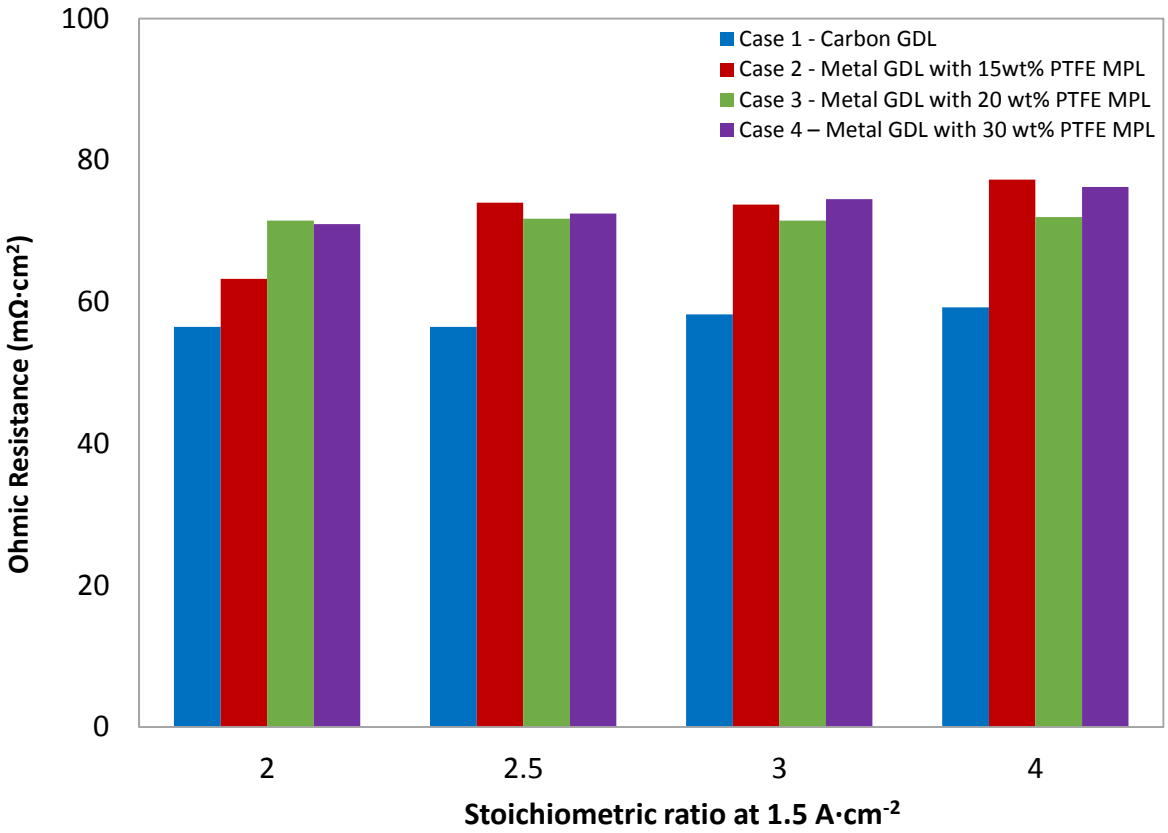

Figure 31: Comparison of ohmic resistances for all cases as a function of cathode flowrate at 1.2 A·cm^{-2}

Similar to the result at 0.25 A·cm^{-2} the ohmic resistances do not change significantly as cathode flowrate increases for all the cases. Figure 31 also shows that the carbon GDL system showed significantly lower ohmic resistance across all cathode flowrates. This is surprising since the contact resistance between the metal GDL and metal flowfield is expected to be less than the contact resistance between the carbon GDL and metal flowfield. The higher ohmic resistance of the metal GDLs suggest that the metal GDL cases are having an effect on the membrane saturation level by either affecting the local temperature at the membrane or by influencing the water balance and movement within the MEA. However, given that the polarisation curves show that the metal GDLs are superior to the carbon GDL the ohmic resistances and therefore the ohmic losses are not the main performance driver at this current density.

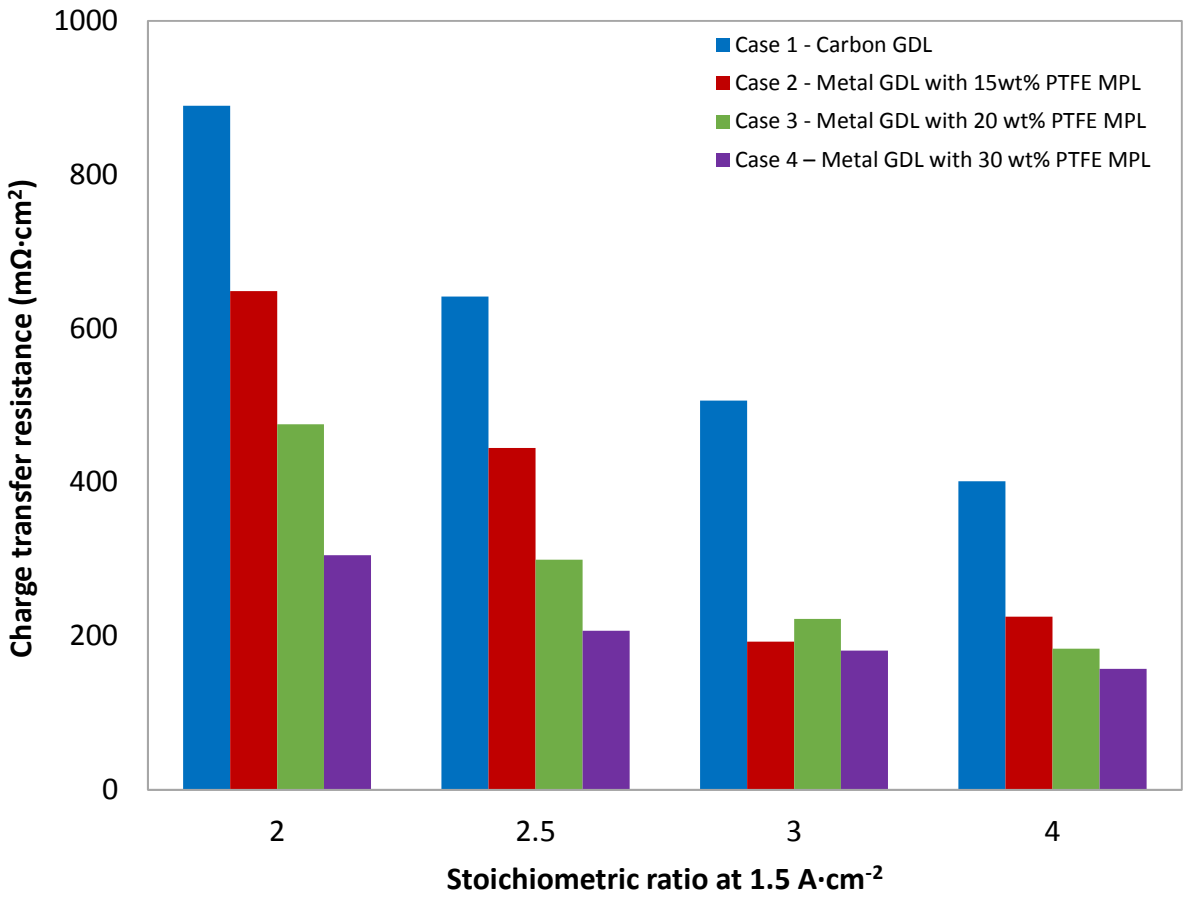

Figure 32: Comparison of charge transfer resistances for all cases as a function of cathode flowrate at 1.2 A·cm^{-2}

Figure 32 shows a decrease in the charge transfer resistance with increasing cathode flowrate for all GDL cases. Since the catalyst layer is constant across all cases, the charge transfer resistance can be used as an indicator of flooding and mass transfer losses as proposed by Cha et al. (2006). The decrease in charge transfer resistance as cathode stoichiometry increases agrees with the polarisation curve results and specifically the trends in limiting current and can therefore be explained with the same arguments.

The carbon GDL case shows a significantly higher charge transfer resistance than all the metal GDL cases at all cathode flowrates indicating significantly more mass transfer limitations. As inferred from Figure 16 these mass transfer limitations are a combination of slow diffusion and water build up both of which result in a lower oxygen concentration in the catalyst layer. For the metal GDL cases only, the general trend is a decreasing charge transfer resistance with an increasing PTFE content in the MPL. This trend is far more pronounced for the lower cathode flowrates. This indicates that the optimum PTFE content in the MPL is very closely linked to the operating conditions such as the operating cathode flowrate. The decreasing charge transfer resistance as PTFE content increases can be explained by recognising that an increase in the PTFE content in the MPL leads to an increase in the

fraction of hydrophobic pores which in turn leads to improved water removal from the catalyst layer. Similar results have been observed in the literature by Park et al. (2008) for carbon GDL based systems.

5.2.3. Two-phase pressure drop coefficient

Figures 33-36 shows the two phase pressure drop coefficients for the different GDL cases as a function of cathode stoichiometric ratio at four different current densities (Tests 6-8). The cathode flowrates were load following (at the stated stoichiometric ratios) and therefore increased as the current density increased.

For all the cases and at all stoichiometric ratios the pressure drop co-efficient increased with decreasing current density. This result is in accordance with the results obtained by Hussaini and Wang (2009) and is explained as follows. At low current densities operating with stoichiometric flows, the cathode flow rate and therefore drag force is less. The reduced drag force limits the ability to remove any liquid water present in the system resulting in pressure build up and subsequently higher pressure drops. Even though at low current densities the amount of liquid water present in the system is less the effect of a reduced drag force is more dominating on the water present in the system.

On comparison of the two phase pressure drop coefficients across various cases, the carbon GDL case shows the highest coefficient values, especially at the lower stoichiometric ratios. This is indicative of water build up in the carbon GDL system resulting from inadequate water removal. The carbon GDL case also arguably shows the most sensitivity to changes in stoichiometric ratio as indicated by the steepness or gradient of the curves. This further suggests significant water build up in the carbon GDL system at the lower stoichiometric ratios. The metal GDL cases with a high PTFE content in the adjacent MPL (20 and 30 wt %) show values very close to unity at the higher stoichiometric ratios. This suggests that the combination of metal GDL, high cathode flowrate and high PTFE content in the MPL allows for excellent water removal from the fuel cell system.

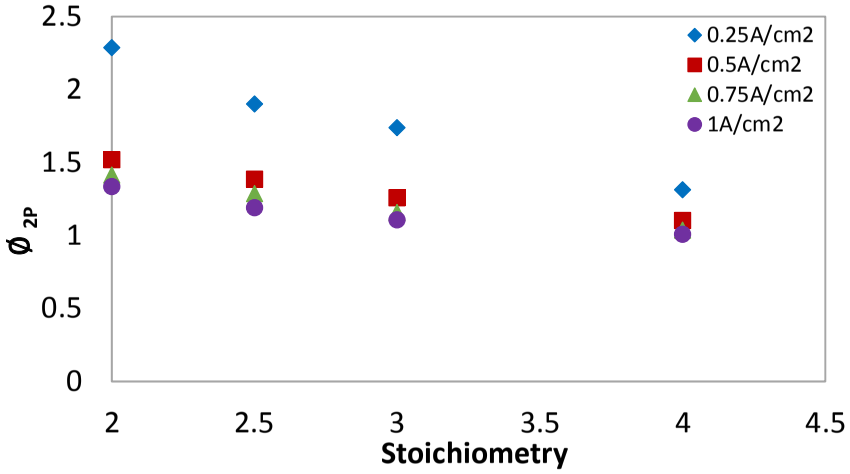

Figure 33: Pressure drop coefficient as function of cathode stoichiometric ratio and current density for carbon GDL

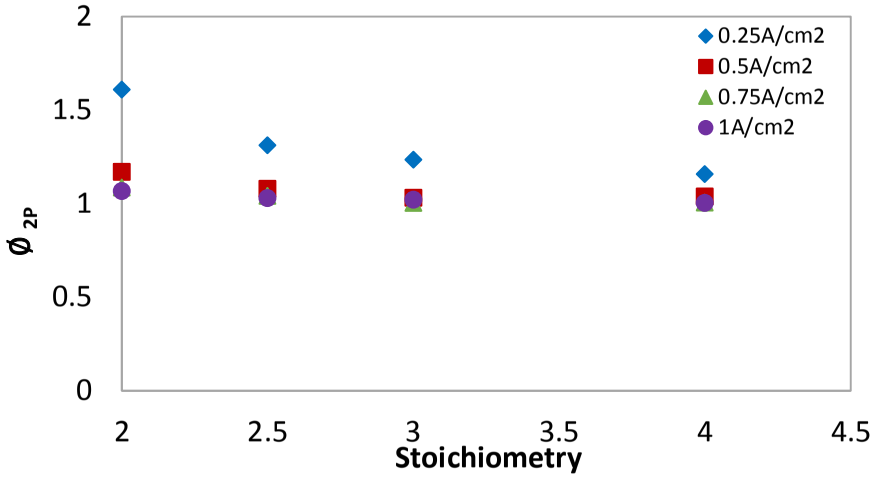

Figure 34: Pressure drop coefficient as function of cathode stoichiometric ratio and current density for Metal GDL with 15wt% PTFE MPL

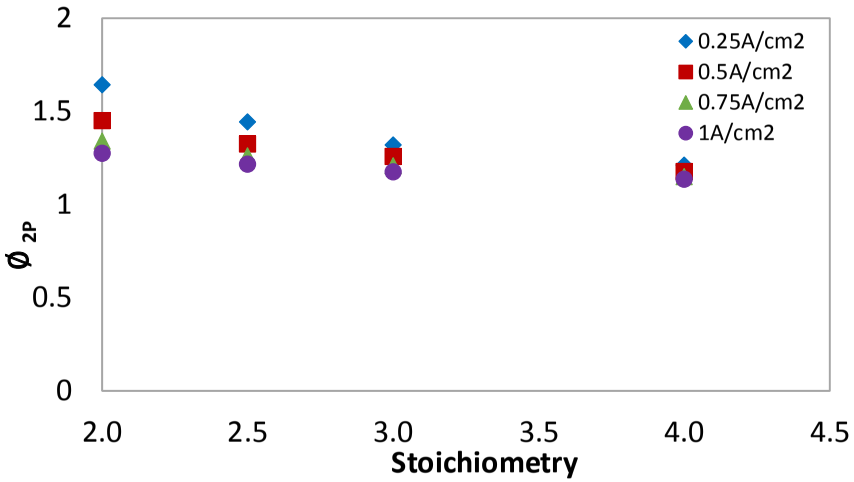

Figure 35: Pressure drop coefficient as function of cathode stoichiometric ratio and current density for Metal GDL with 20wt% PTFE MPL

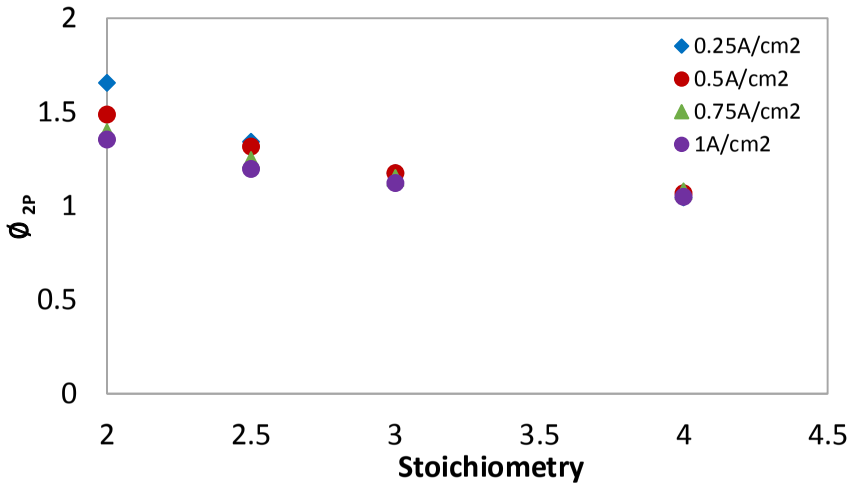

Figure 36: Pressure drop coefficient as function of cathode stoichiometric ratio and current density for Metal GDL with 30wt% PTFE MPL

5.2.4. Voltage stability tests

Figures 37- 40 and Figures 41-44 show the results of the voltage stability tests for the different GDL cases as a function of cathode stoichiometric ratio at 0.25 $A \cdot cm^{-2}$ and 1 $A \cdot cm^{-2}$ respectively (Tests 6-8).

In general, for all GDL cases at 0.25$A \cdot cm^{-2}$ and at all stoichiometric ratios apart from the lowest value of 2, the cell voltage remained relatively constant over the time period tested. This result is not surprising since the combination of a low operating current density and therefore low rate of water production together with a high drag force reduces the probability significant water build-up and subsequently flooding. One anomaly to this trend is the metal GDL with 15wt% PTFE case at a stoichiometric ratio of 2.5. The cell voltage appears slightly unstable and a sharp drop in voltage was observed at approximately 6000s indicating some water build up and discharge at these conditions. At the lowest stoichiometric ratio of 2, there are small voltage fluctuations for the majority of cases which points to small amounts of water build up.

The results at 1 $A \cdot cm^{-2}$ are more revealing in terms of which of the cases experience flooding. For the carbon GDL case, the cell voltage shows many sharp downward spikes over the time interval observed. These downward peaks are due to a build-up of water in the cell which blocks the gas pathways in the cell and leads to temporary severe flooding. The downward peaks becomes less frequent and reduce in magnitude as the cathode stoichiometric ratio increases. The increased stoichiometric ratio increases the drag force which in turn reduces the possibility of liquid water build up.

In comparison to the carbon GDL case all the metal GDL cases at 1$A \cdot cm^{-2}$ displayed very small to no downward peaks at all stoichiometric ratios. This indicates no severe flooding for the metal GDL cases. At a stoichiometric ratio of 2 all the metal GDL cases show some voltage instability indicating a degree of water build up. The metal GDL case with 15 wt% PTFE in the MPL shows some voltage instability at all stoichiometric ratios. Whist no severe flooding is taking place this suggests a PTFE content of 15wt% is on the low side in terms of adequate water removal at the operating conditions used in this study.

Overall the voltage stability tests show less water building and flooding for the metal GDL cases with a high PTFE content in the MPL (20 and 30 wt%).

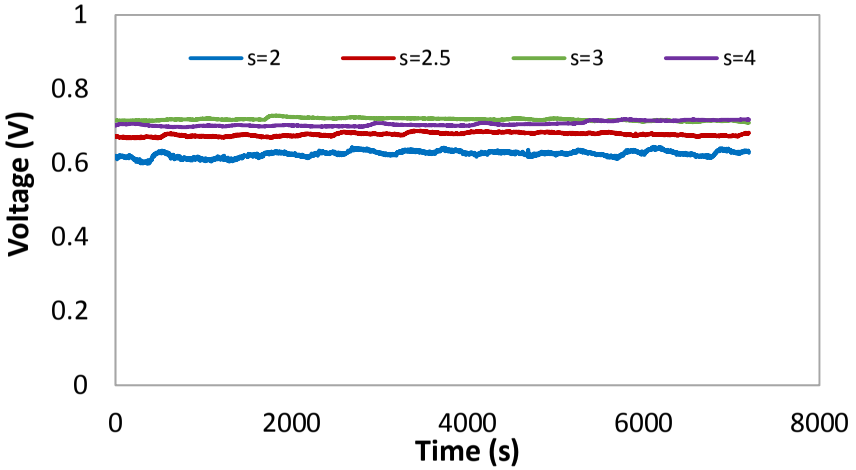

Figure 37: Cell voltage at different cathode stoichiometric ratios for carbon GDL at 0.25 A·cm^{-2}

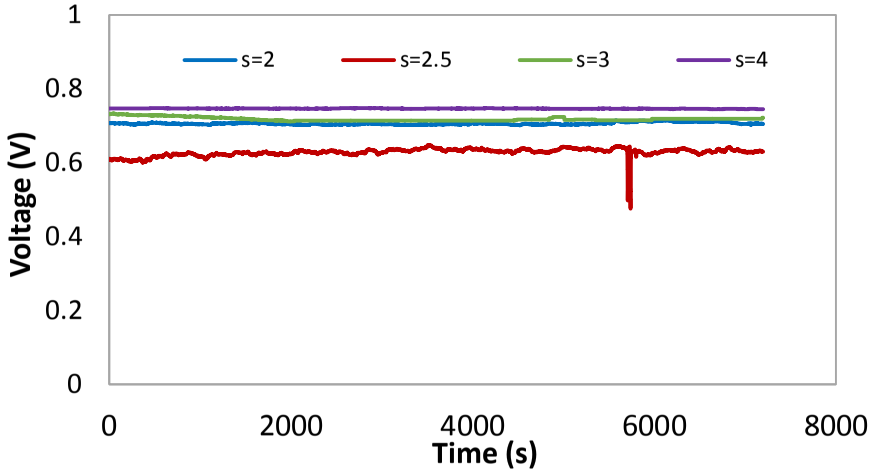

Figure 38: Cell voltage at different cathode stoichiometric ratios for Metal GDL with 15wt% PTFE MPL at 0.25 A·cm^{-2}

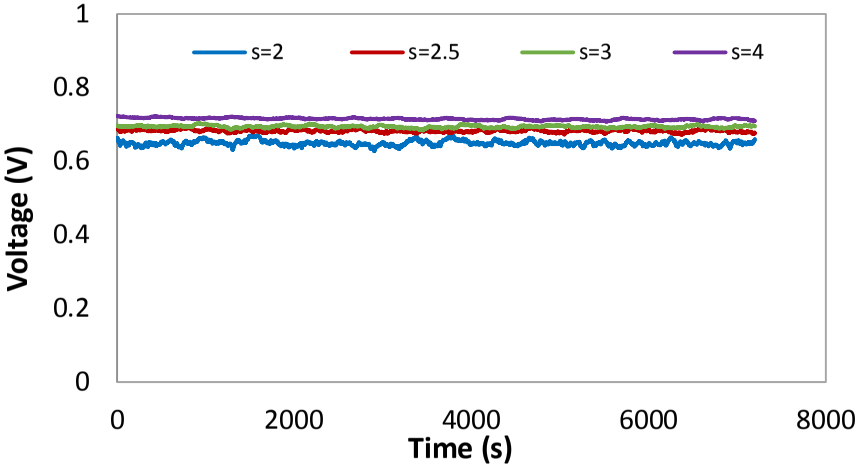

Figure 39: Cell voltage at different cathode stoichiometric ratios for Metal GDL with 20wt% PTFE MPL at 0.25 A·cm^{-2}

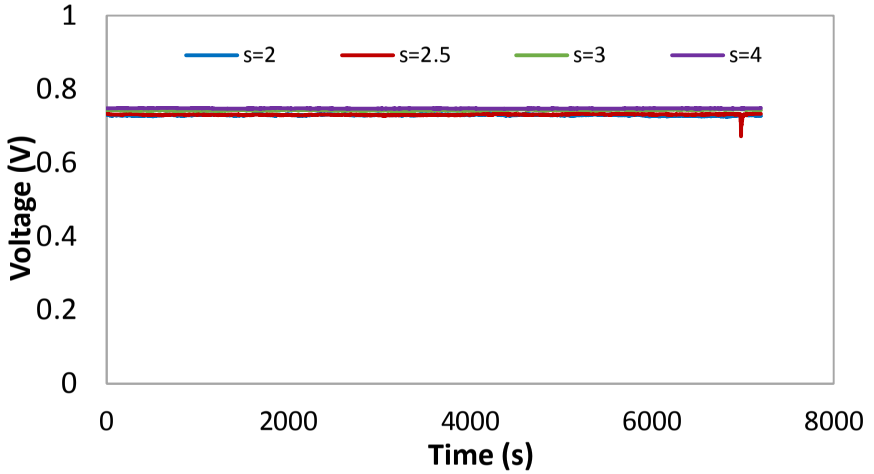

Figure 40: Cell voltage at different cathode stoichiometric ratios for Metal GDL with 30wt% PTFE MPL at 0.25 A·cm^{-2}

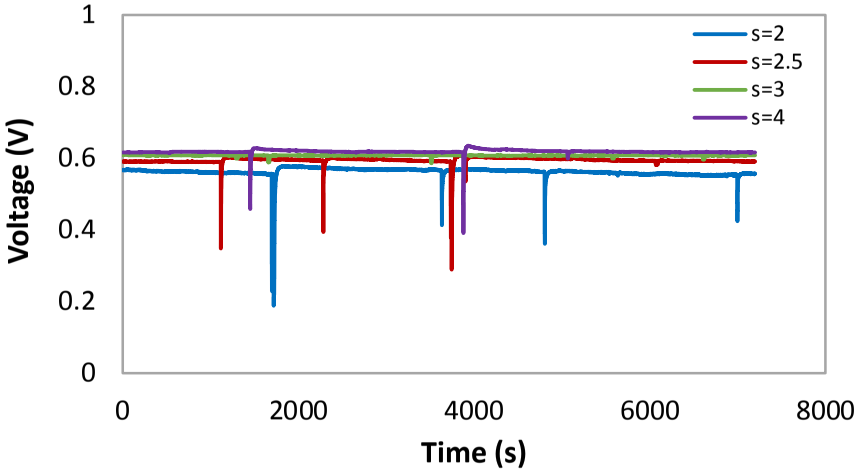

Figure 41: Cell voltage at different cathode stoichiometric ratios for carbon GDL at 1 A·cm^{-2}

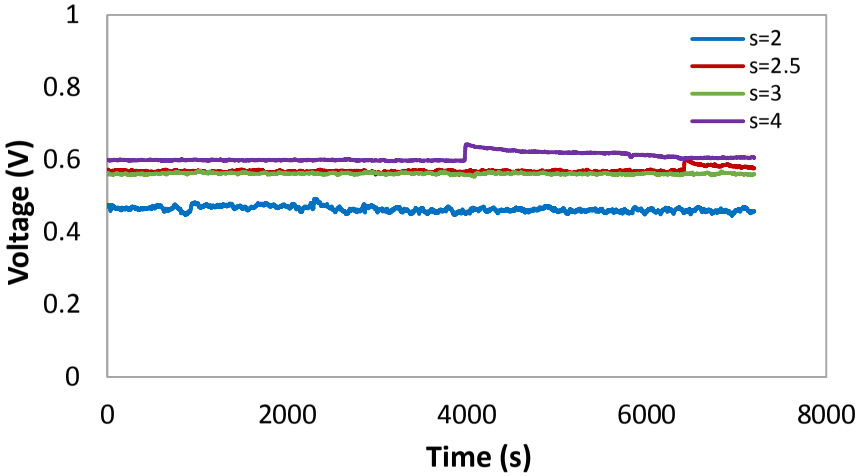

Figure 42: Cell voltage at different cathode stoichiometric ratios for Metal GDL with 15wt% PTFE MPL 1 A·cm^{-2}

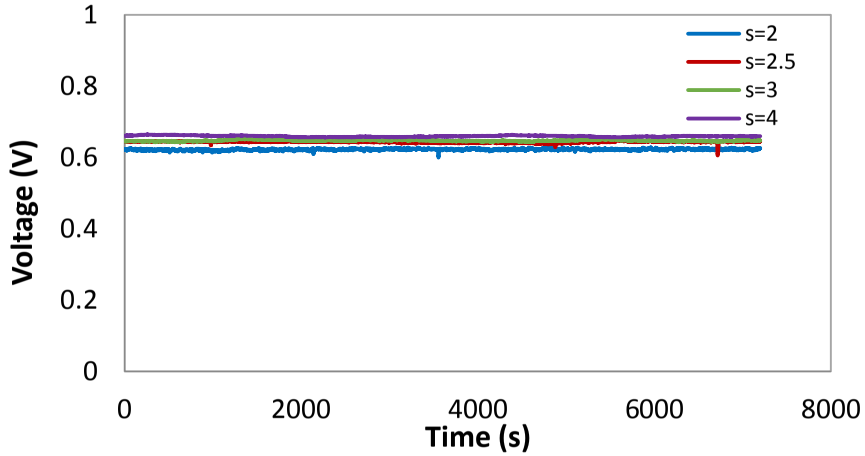

Figure 43: Cell voltage at different cathode stoichiometric ratios for Metal GDL with 20wt% PTFE MPL at 1 A·cm^{-2}

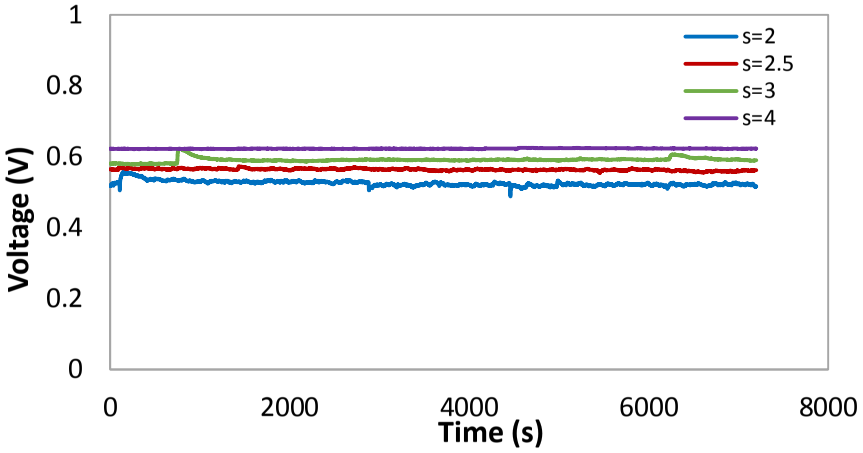

Figure 44: Cell voltage at different cathode stoichiometric ratios for Metal GDL with 30wt% PTFE MPL at 1 A·cm-2

6. Conclusions

From the investigation into the manipulation of operating conditions, it was confirmed that increasing the cathode flowrate is a viable water management strategy as it assists with the removal of liquid water. This increase in performance was attributed to both an increase in oxygen partial pressure as well as an increase in the drag force available to expel excess water from the cell. Furthermore, the results from the study suggest that both these effects contribute equally to the effects observed thereby confirming that increasing the cathode flowrate is a viable water management strategy as it assists with the removal of liquid water.

The second water management strategy investigated looked into the effect of altering the cathode GDL from a conventional carbon paper GDL to a metal GDL with varying MPL hydrophobicity values. The overall results obtained suggest that the metal GDLs with high MPL PTFE contents (20 and 30 wt.%) showed the best overall performance and water management of all the cases tested. The performance limiting current results showed a general increase for increasing PTFE content. It showed however be noted that too high a PTFE content may lead to resistance to gas flow due to less porosity.

The improved water management was observed in the high current density region using the results obtained by the EIS, two phase pressure coefficient and voltage stability tests. These test results all showed that the increased PTFE content assisted with the removal of liquid water and prevented fuel cell flooding. It should also be highlighted that at high current densities, the charge transfer resistances for the metal GDL cases indicated that the optimum PTFE content in the MPL was closely linked to the operating conditions such as the operating cathode flowrate.

It is important to note that the results of this study were specifically made for PEFCs using metal flowfield plates with a straight parallel microchannel channel design. The performance results may be significantly altered should any of the components change.

The following recommendations are made for further investigation:

- To fully characterise the MPL to help create a better understanding of the observations made in this study. Characterisation techniques of the MPL could include mercury porosimetry and gas permeability tests
- To investigate the effect of the MPL thickness on the water management of the fuel cell

7. Reference

Alaefour, I., Karimi, G., Jiao, K., Shakhshir, S.A. & Li, X. 2011. Experimental study on the effect of reactant flow arrangements on the current distribution in proton exchange membrane fuel cells. *Electrochimica Acta.* 56(5):2591-2598. DOI:http://dx.doi.org.ezproxy.uct.ac.za/10.1016/j.electacta.2010.11.002.

Baker, R. & Zhang, J. 2011. *Polymer Electrolyte Membrane (PEM) Fuel Cells.* Available: http://electrochem.cwru.edu/encycl/art-f04-fuel-cells-pem.htm.

Barbir, F. 2005. PEM Fuel Cells: Theory and Practice. In Elsevier Inc. 122-123.

Barbir, F. 2006. *Fuel Cell Technology: Reaching towards commercialzation.* Springer London.

Barbir, F., Husar, A., & Venkataraman, R., 2001. Pressure drop as a diagnostic tool for PEM fuel cells, *Electrochemical Society's Fall Meeting*, San Francisco

Barbir, F., Gorgun, H. & Wang, X. 2005. Relationship between pressure drop and cell resistance as a diagnostic tool for PEM fuel cells. *Journal of Power Sources.* 141:96-101.

Barbir, F. & Yazici, S., 2007. Status and development of PEM fuel cell technology. *International Journal of Energy Research*, (38), 369-78.

Bazylak, A. 2009. Liquid water visualization in PEM fuel cells: A review. *International Journal of Hydrogen Energy.* 34:3845-3857.

Bazylak, A., Sinton, D., Liu, Z.S. & Djilali, N. 2007. Effect of compression on liquid water transport and microstructure of PEMFC gas diffusion layers. *Journal of Power Sources.* 163:784-792.

Bhatt, S., Gupta, B., Sethi, V.K. & Pandey, M. 2012. Polymer Exchange Membrane (PEM) Fuel Cell: A Review. *International Journal of Current Engineering and Technology.* 2(1).

Blanco, M., Wilkinson, D.P., Wang, H. & Liu, S.Z.S., 2008. Engineered Gas Diffusion Layers for PEM Fuel Cells. *The Electrochemical Society.* :218.

Cha, S.W., O'Hayre, R., Park, Y. & Prinz, F.B. 2006. Electrochemical impedance investigation of flooding in micro-flow channels for proton exchange membrane fuel cells. *Journal of Power Sources.* 161:138-142.

Chang, J., Kuan, Y. & Lee, S. 2014. Experimental Investigation of a Direct Methanol Fuel Cell with Hilbert Fractal Current Collectors*. Journal of Chemistry*. Article ID 371616. doi:10.1155/2014/371616

Diep, J. et al., 2007. Development of a residence time distribution method for proton exchange membrane fuel cell evaluation. *Chemical Engineering Science,* 62(3), pp.846–857.

Eikerling, M. & Kornyshev, A.A. 1998. Modelling the performance of the cathode catalyst layer of polymer electrolyte fuel cells. *Journal of Electroanalytical Chemistry.* 453:89-106.

Elsevier 2014. Available: http://www.journals.elsevier.com/journal-of-power-sources/ [2014, February 25].

Feindel, K.W., Bergens, S.H. & Wasylishen, R.E. 2006. The use of 1H NMR microscopy to study proton-exchange membrane fuel cells. *Physical Chemistry Chemical Physics.* 7:67-75.

Feindel, K.W., Bergens, S.H. & Wasylishen, R.E. 2007. The influence of membrane electrode assembly water content on the performance of a polymer electrolyte membrane fuel cell as investigated by 1H NMR microscopy. *Physical Chemistry Chemical Physics.* 9:1850-1857.

Freire, T.J. & Gonzalz, E.R. 2001. Effect of membrane characteristics and humidification conditions on the impedance responsse of polymer electrolyte fuel cells. *Journal of Electroanalytical Chemistry.* 503:57-68.

FuelCellsEtc 2013. *Comparing Gas Diffusion Layers.* Available: http://fuelcellsetc.com/2013/03/comparing-gas-diffusion-layers-gdl/.

Fushinobu, K., Takahashi, D. & Okazaki, K. 2006. Micromachined metallic thin films for the gas diffusion layer of PEFCs. *Journal of Power Sources.* 158(2):1240-1245. DOI:http://dx.doi.org.ezproxy.uct.ac.za/10.1016/j.jpowsour.2005.10.080.

Gebregergis, A., Pillay, P. & Rengaswamy, R. 2010. PEMFC Fault Diagnosis, Modeling, and Mitigation. *Ieee Transactions on Industry Applications.* 46(1):295-303.

Gostick, J.T., Fowler, M.W., Loannidis, M.A., Pritzker, M.D., Volfkovich, Y.M. & Sakars, A. 2006. *Journal of Power Sources.* 156:375.

Hakenjos, A., Muenter, H., Wittstadt, U. & Hebling, C.A. 2004. PEM fuel cell for combined measurement of current and temperature distribution, and flow field flooding. *Journal of Power Sources.* 131:213-216.

He, W., Lin, G. & Nguyen, T.V., 2003. Diagnostic tool to detect electrode flooding in Proton-Exchange-Membrane Fuel Cells. AIChE Journal. 49 (12). 3221–3228

Hussaini, I.S. & Wang, C.Y. 2009. Visualization and quantification of cathode channel flooding in PEM fuel cells. *Journal of Power Sources.* 187:444-451.

International Society of Electrochemistry 2013. *Impact Factor 2012 of Electrochemistry Journals.* Available: http://www.ise-online.org/popup/Impact_Factor_2012.pdf [2014, February 24].

Jayakumar, A., Sethu, S.P., Ramos, M., Robertson, J. & Al-Jumaily, A. 2014. A technical review on gas diffusion, mechanism and medium of PEM fuel cell. *Springer.* 21:1-18.

Ji, M. & Wei, Z. 2009. A Review of Water Management in Polymer Electrolyte Membrane Fuel Cells. *Energies.* 2:1057-1106.

Kumbur, E.C. & Mench, M.M. 2009. Fuel Cells – Proton-Exchange Membrane Fuel Cells | Water Management. *Elsevier.* 828-846.

Kwac, L.K. & Kim, H.G. 2008. Investigation of gas flow characteristics in proton exchange membrane fuel cell. *Journal of Mechanical Science and Technology.* 22:1561-1567.

Larminie, J. & DIcks, A. Fuel Cell Systems Explained. In Second Edition ed. John Wiley & Sons Ltd.

Le Canut, J., Abouatallah, R.M. & Harrington, D.A. 2006. Detection of Membrane Drying, Fuel Cell Flooding, and Anode Catalyst Poisoning on PEMFC Stacks by Electrochemical Impedance Spectroscopy. *Journal of the Electrochemical Society.* 153(5):A857-A864.

Lee, W. K., & Zee, J. W. Van. (1999). Effect of humidity on PEM Fuel Cell Performance Part I – Experiments

Li, H., Tang, Y., Wang, Z., Shi, Z., Wu, S., Songa, D., Zhang, J., Fatih, K. 2008. A review of water flooding issues in the proton exchange membrane fuel cell. *Journal of Power Sources.* 178:103-117.

Li, X.G., Sabir, I. & Park, J. 2007. A channel design procedure for PEM fuel cells with effective water removal. *Journal of Power Sources.* 163:933-942.

Litster, S., Buie, C.R., Fabian, T., Eaton, J.K. & Santiago, J.G. 2007. Active Water Management for PEM Fuel Cells. *Journal of the Electrochemical Society.* 54(10):B1049-B1058.

Marklines 2005. *Fuel Cell Technology Advancing in Fields Such as Non-fluorinated Electrolytes and Molded Separators.* Available: http://www.marklines.com/en/report/rep347_200502.

Mathias, M.F., Roth, J., Fleming, J., Lehnert, W., Vielstich, W. & Gasteiger, H.A. 2003. *Handbook of Fuel Cells—Fundamentals,Technology and Applications.* New York: John Wiley & Sons.

Mehta, V. & Cooper, J.S. 2002. Review and analysis of PEM fuel cell design and manufacturing. *Journal of Power Sources.* 14:32-53.

Merida, W.R., McLean, G. & Djilali, N. 2006. Non-planar architecture for proton exchange membrane fuel cells. *Journal of Power Sources.* 162:415-425.

Morin, A., Xu, F., Gebel, G. & Diat, O. 2010. Influence of PEMFC gas flow configuration on performance and water distribution studied by SANS: Evidence of the effect of gravity. *International Journal of Hydrogen Energy.* 36:3096-3109.

Nam, J.H. & Kaviany, M. 2003. Effective diffusivity and water-saturation distribution in single- and two-layer PEMFC diffusion medium. *International Journal of Heat and Mass Transfer.* 46:4595-4611.

Nam, J.H., Lee, K.J., Hwang, G.S., Kim, C.J. & Kaviany, M. 2009. Microporous layer for water morphology control in PEMFC. *International Journal of Heat and Mass Transfer.* 52:2779-2791.

Nguyen, T.V. 1996. A gas distributor design for proton-exchange membrane fuel cells. *Journal of the Electrochemical Society.* 143:L103-L105.

Nguyen, T.V. 2006. Water Management by Material Design and Engineering for PEM Fuel Cells. *ECS Trans.* 3:1171.

Nishidaa, K., Taniguchia, R., Ishizakia, Y., Tsushimab, S. & Hiraic, S. 2015. Impacts of channel wettability and flow direction on liquid water transport in the serpentine flow field of a polymer electrolyte fuel cell. *Journal of Power Sources.* 275:447-457.

Park, S., Lee, J. & Popov, B.N. 2008. Effect of PTFE content in microporous layer on water management in PEM fuel cells. *Journal of Power Sources*. 177(2):457-463. DOI:http://dx.doi.org/10.1016/j.jpowsour.2007.11.055.

Park, S., Lee, J., & Popov, B.N. 2012. A review of the gas diffusion layer in PEM fuel cells: Materials and designs. *International Journal of Hydrogen Energy.* 37:5850-5865.

'Siefert, N.S.'. & 'Litster, S. 2011. Voltage loss and fluctuation in proton exchange membrane fuel cells: The role of cathode channel plurality and air stoichiometric ratio. 196(4):1948-1948-1954.

Soler, J., Hontanon & Daza, L. 2003. Electrode permeability and flow-field confirguration: influence on the performance of a PEMFC. *Journal of Power Sources.* 118:172-178.

Spernjak, D., Prasad, A.K. & Advani, S.G. 2007. Experimental investigation of liquid water formation and transport in a transparent single-serpentine PEM fuel cell. *Journal of Power Sources.* 170:334-344.

Stumper, J., Löhr, M. & Hamada, S. 2005. Diagnostic tools for liquid water in PEM fuel cell. *Journal of Power Sources.* 143:150-157.

Thomson Reuters 2014. *Citation Report: 1.* Available: http://apps.webofknowledge.com/CitationReport.do?product=UA&search_mode=CitationReport&SID=N1P1DoheYN2OwVbBtRM&page=1&cr_pqid=1&viewType=summary [2014, February 25].

Tsushima, S., Teranishi, K. & Hirai, S. 2004. Magnetic resonance imaging of the water distribution within a polymer electrolyte membrane in fuel cells. *Electrochemical and Solid-State Letters.* 7:A269-A272.

Tüber, K., Pócza, D. & Hebling, C. 2003. Visualization of water buildup in the cathode of a transparent PEM fuel cell. *Journal of Power Sources.* 124:403-414.

Watanabe, M., Satoh, Y. & Shimura, C. 1993. Management of the water content in polymer electrolyte membranes with porous fiber wicks. 140:3190-3193.

Watanabe, M., Uchida, H., Seki, Y. & Emori, M. 1996. Self-humidifying polymer electrolyte membranes for fuel cells. *Journal of the Electrochemical Society.* 143:3847-3852.

Wood, D.L., Yi, J.S. & Nguyen, T.V. 1998. Effect of direct liquid wtare injection and interdigitated flowfield on the performance of proton exchange membrane fuel cells. *Elelctrochim. Acta.* 43:3795-3809.

Xue, D. & Dong, Z. 1998. Optimal Fuel Cell System Design Considering Functional Performance and Production Costs. *Journal of Power Sources.* 76:69-80.

Yuan, X.-.R., Song, C., Wang, H. & Zhang, J. 2010. Electrochemical Impedance Spectroscopy in PEM Fuel Cells. In Springer-Verlag London.

Zhang, F.Y., Advani, S.G. & Prasad, A.K., 2008. Performance of a metallic gas diffusion layer for PEM fuel cells. *Journal of Power Sources.* 176:293-298.

Zhang, J., Li, H., Shi, Z. & Zhang, J. 2010. Effects of hardware design and operation conditions on PEM fuel cell water flooding. *International Journal of Green Energy.* 7(5):461-474.

8. Appendix

8.1. Appendix 1

Table A1: Summary of the various cases investigated

Case	GDL material	GDL manufacturer	GDL thickness (µm)	GDL description	MPL PTFE content (wt%)
1	Carbon	Freudenberg Fuel Cell Component Technologies	210	• Carbon paper with 5wt% bulk hydrophobic treatment. • Product code: H2315 I6	20
2	Metal - stainless steel	Toyo Precision Parts MFG Co. Ltd	30	• Perforated metal sheet with hole diameter of 60 µm and pitch of 110 µm • Surface treated with 1 µm gold coating • No bulk hydrophobic treatment	15
3					20
4					30

Table A2: Summary of tests and operating conditions

Test No.	Experimental case (Table 1)	Operating conditions						Diagnostic tests performed
		T (°C)	P (bar)	RH (%)	S_{anode}	$S_{cathode}$	Cf/Lf	
1	1	80	1	100	1.5 at 1.5 $A \cdot cm^{-2}$	2, 2.5, 3, 4 at 1.5 $A \cdot cm^{-2}$	Cf	• Polarisation curves • EIS
2	2							
3	3							
4	4							
5	1				1.5	2, 2.5, 3, 4	Lf	• Two phase pressure drop coefficient tests • Voltage stability tests
6	2							
7	3							
8	4							
9	1		a = 1, c = varying*		1.5	2	varying *	• Polarisation curves

Cf = constant flow, Lf= Load following

**Procedure described in Section 4.4.2 - cathode stoichiometry investigation*

8.2. Appendix 2

8.2.1. Sample calculations

The sample calculations shown in this section was done at a current density of 1.5 A·cm^{-2}.

Calculations used to determine the feed volumetric flow of Hydrogen gas required

The number of moles of gas consumed at targeted current density can be calculated as follows:

$$\dot{n}_{H2\ consumed} = \frac{iA}{2\ F}$$

$$\dot{n}_{H2\ consumed} = \frac{(1.5)(25)}{2\ (96490)}$$

$$\dot{n}_{H2\ consumed} = 1.94x10^{-4}\ mol \cdot s^{-1}$$

Using the anode stoichiometric ratio 1.5, the molar flowrate becomes:

$$\dot{n}_{H2(at\ s=1.5)} = 1.5\ (\dot{n}_{H2\ consumed})$$

$$\dot{n}_{H2(at\ s=1.5)} = 1.5\ (1.94x10^{-4}\ mol \cdot s^{-1})$$

$$\dot{n}_{H2(at\ s=1.5)} = 2.92x10^{-4}\ mol \cdot s^{-1}$$

The ideal gas equation was then used at a temperature of 273.15K and 1Bara to determine the feed volumetric flowrate required.

$$V_{H2} = \frac{\dot{n}_{o2(at\ s=1.5)}\ RT}{P}$$

$$V_{H2} = \frac{(2.92x10^{-4})(8.314)(273.15)}{1 * 101325}$$

$$V_{H2} \doteq 6.53\ x10^{-6}\ m^3 \cdot s^{-1}$$

$$V_{H2} = \ 0.4\ \ l \cdot min^{-1}$$

Calculations used to determine the feed volumetric flow of Air required

The number of moles of gas consumed at targeted current density can be calculated as follows:

$$\dot{n}_{O2\ consumed} = \frac{iA}{4\ F}$$

$$\dot{n}_{O2\ consumed} = \frac{(1.5)(25)}{4\ (96490)}$$

$$\dot{n}_{O2\ consumed} = 9.72x10^{-5}\ mol \cdot s^{-1}$$

Using the anode stoichiometric ratio 2, the molar flowrate becomes:

$$\dot{n}_{O2(at\ s=2)} = 2\ (\dot{n}_{H2\ consumed})$$

$$\dot{n}_{O2(at\ s=2)} = 2\ (9.72x10^{-5} mol \cdot s^{-1})$$

$$\dot{n}_{O2(at\ s=2)} = 1.94x10^{-5}\ mol \cdot s^{-1}$$

The molar flowrate of air required was calculated as follows:

$$\dot{n}_{Air} = \frac{\dot{n}_{O2(at\ s=2)}}{0.21}$$

$$\dot{n}_{Air} = \frac{1.94x10^{-5}}{0.21}$$

$$\dot{n}_{Air} = 9.25x10^{-5}\ mol \cdot s^{-1}$$

The ideal gas equation was then used at a temperature of 273.15K and 1Bara to determine the feed volumetric flowrate required.

$$\dot{V}_{Air} = \frac{\dot{n}_{Air} RT}{P}$$

$$\dot{V}_{Air} = \frac{(9.25x10^{-5})(8.314)(273.15)}{1 * 101325}$$

$$\dot{V}_{Air} = 2.07\ x10^{-5}\ m^3 \cdot s^{-1}$$

$$\dot{V}_{Air} = 1.25\ l \cdot min^{-1}$$

EBE Faculty: Assessment of Ethics in Research Projects

Any person planning to undertake research in the Faculty of Engineering and the Built Environment at the University of Cape Town is required to complete this form before collecting or analysing data. When completed it should be submitted to the supervisor (where applicable) and from there to the Head of Department. If any of the questions below have been answered YES, and the applicant is NOT a fourth year student, the Head should forward this form for approval by the Faculty EIR committee: submit to Ms Zakiya Chikte (Zakiya.chikte@uct.ac.za); New EBE Building, Ph 021 650 5739). Students must include a copy of the completed form with the dissertation/thesis when it is submitted for examination.

Name of Principal Researcher/Student: Simone Daniels Department: Chemical Engineering

If a Student: Degree: MSc Engineering (Chemical) Supervisor: Mr Nabeel Hussain

If a Research Contract indicate source of funding/sponsorship:

Research Project Title: Water management strategies for Polymer Electrolyte Fuel Cells (PEFCs) employing microchannel flowfields

Overview of ethics issues in your research project:

Question 1: Is there a possibility that your research could cause harm to a third party (i.e. a person not involved in your project)?	YES	NO ✓
Question 2: Is your research making use of human subjects as sources of data? If your answer is YES, please complete Addendum 2.	YES	NO ✓
Question 3: Does your research involve the participation of or provision of services to communities? If your answer is YES, please complete Addendum 3.	YES	NO ✓
Question 4: If your research is sponsored, is there any potential for conflicts of interest? If your answer is YES, please complete Addendum 4.	YES	NO ✓

If you have answered YES to any of the above questions, please append a copy of your research proposal, as well as any interview schedules or questionnaires (Addendum 1) and please complete further addenda as appropriate.

I hereby undertake to carry out my research in such a way that

- there is no apparent legal objection to the nature or the method of research; and
- the research will not compromise staff or students or the other responsibilities of the University;
- the stated objective will be achieved, and the findings will have a high degree of validity;
- limitations and alternative interpretations will be considered;
- the findings could be subject to peer review and publicly available; and
- I will comply with the conventions of copyright and avoid any practice that would constitute plagiarism.

Signed by:

	Full name and signature	Date
Principal Researcher/Student:	Simone Daniels 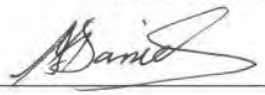	27-08-2015

This application is approved by:

Supervisor (if applicable):	NABEEL HUSSAIN	27.08.2015
HOD (or delegated nominee): Final authority for all assessments with NO to all questions and for all undergraduate research.		27-8-2015
Chair : Faculty EIR Committee For applicants other than undergraduate students who have answered YES to any of the above questions.		